



**HAL**  
open science

## Directing the solid-state photochromic and luminescent behaviors of spiromolecules with Dawson and Anderson polyoxometalate units

Hachem Dridi, Amandine Boulmier, Patricia Bolle, Anne Dolbecq, Jean-Noël Rebilly, Frédéric Banse, Laurent Ruhlmann, Hélène Sérrier-Brault, Remi Dessapt, Pierre Mialane, et al.

### ► To cite this version:

Hachem Dridi, Amandine Boulmier, Patricia Bolle, Anne Dolbecq, Jean-Noël Rebilly, et al.. Directing the solid-state photochromic and luminescent behaviors of spiromolecules with Dawson and Anderson polyoxometalate units. *Journal of Materials Chemistry C*, 2020, 8 (2), pp.637-649. 10.1039/c9tc05906g . hal-02572108

**HAL Id: hal-02572108**

**<https://hal.science/hal-02572108>**

Submitted on 13 May 2020

**HAL** is a multi-disciplinary open access archive for the deposit and dissemination of scientific research documents, whether they are published or not. The documents may come from teaching and research institutions in France or abroad, or from public or private research centers.

L'archive ouverte pluridisciplinaire **HAL**, est destinée au dépôt et à la diffusion de documents scientifiques de niveau recherche, publiés ou non, émanant des établissements d'enseignement et de recherche français ou étrangers, des laboratoires publics ou privés.



## Directing the solid-state photochromic and luminescent behaviors of spiromolecules with Dawson and Anderson polyoxometalate units.

Received 00th January 20xx,  
Accepted 00th January 20xx

DOI: 10.1039/x0xx00000x

www.rsc.org/

Hachem Dridi,<sup>‡ab</sup> Amandine Boulmier,<sup>‡a</sup> Patrica Bolle,<sup>c</sup> Anne Dolbecq,<sup>a</sup> Jean-Nöel Reilly,<sup>b</sup> Frédéric Banse,<sup>b</sup> Laurent Ruhlmann,<sup>\*d</sup> Hélène Serier-Brault,<sup>c</sup> Rémi Dessapt,<sup>\*c</sup> Pierre Mialane,<sup>a</sup> and Olivier Oms<sup>\*a</sup>

A series of three new polyoxometalate/spiromolecules compounds – including the **(TBA)<sub>3</sub>[AlMo<sub>6</sub>-SN]** (SN = spironaphthoxazine) and **(TBA)<sub>3</sub>[AlMo<sub>6</sub>-SP]** (SP = spiropyran) Anderson-type polyoxometalates (POMs) and the unprecedented **(TBA)<sub>5</sub>[P<sub>2</sub>W<sub>15</sub>V<sub>3</sub>-SP]** Dawson-type species – has been synthesized and characterized using a full panel of techniques. These hybrids have been thoroughly investigated by (spectro)electrochemical techniques, allowing not only to extract the electrochemical data characterizing these POMs but also to deeply investigate the redox mechanisms involved, including the dimerization process occurring during the oxidation step. The solid-state photochromic properties of these species have been fully studied and the photochromic kinetic parameters determined. It revealed that while in **(TBA)<sub>5</sub>[P<sub>2</sub>W<sub>15</sub>V<sub>3</sub>-SP]** the merocyanin form is highly stabilized, **(TBA)<sub>3</sub>[AlMo<sub>6</sub>-SN]** represents highly robust optical switch. Importantly, the room temperature solid-state luminescent properties of such assemblies have been investigated for the first time. It has been evidenced that **(TBA)<sub>3</sub>[AlMo<sub>6</sub>-SP]** exhibits a strong red emission under UV irradiation, while the luminescence of the related **(TBA)<sub>3</sub>[MnMo<sub>6</sub>-SP]** is weaker and that **(TBA)<sub>5</sub>[P<sub>2</sub>W<sub>15</sub>V<sub>3</sub>-SP]** does not exhibit luminescent properties. These emission intensity differences have been interpreted in terms of differences in photoinduced electron transfers from the excited state of the merocyanine isomer to the inorganic units. A correlation between its efficiency and the electron acceptor ability of the POMs determined from electronic absorption spectroscopic measurement and electrochemical data has been proposed.

### Introduction

Photochromic materials able to reversibly change color under light stimulus are still of increasing interest due to their promising and marketable applications in optical sensors<sup>1</sup> such as data recording and storage,<sup>2</sup> photo-controlled biological systems,<sup>3</sup> molecular logic gates,<sup>4</sup> electrochemical wiring<sup>5</sup> and sunglasses.<sup>6</sup> Generally, these systems require strong photocoloration contrast, fast and reversible switching process and high photofatigue resistance. Among all the classical UV-activated photochromes (azobenzenes,<sup>7</sup> diarylethenes,<sup>8</sup> fulgides,<sup>9</sup> ...), spiropyrans have a special place due to their specific

properties.<sup>10</sup> These molecules in their colorless closed form (SP) are composed of perpendicular indoline and chromene rings bound together *via* a spiro junction. Under UV irradiation, the C<sub>spiro</sub>-O bond can be cleaved and the SP form is converted to the highly colored planar merocyanine (MC) isomer (Scheme 1). The photoisomerization is reversible and the initial SP form can be recovered by irradiating the MC isomer under visible light. The SP→MC switching process induces a strong change of the physico-chemical properties (hydrophilicity, coordinating ability) along with a huge conformational reorganization. Moreover the equilibrium between the two forms is also sensitive to many others stimuli: solvent,<sup>11</sup> temperature,<sup>12</sup> acidity,<sup>13</sup> metal ions<sup>14</sup> and mechanical force,<sup>15</sup> which makes this photochrome unique. Most of the reported spiropyran-based optical devices consist on the immobilization of the molecular switch onto various supports including polymer matrices,<sup>16</sup> surfaces,<sup>17</sup> nanoparticles,<sup>18</sup> silica network<sup>19</sup> and metal-organic frameworks.<sup>20</sup> As a matter of fact, although spiropyran derivatives exhibit strong photochromism in solution, there are only a few examples of solid-state photochromic compounds at room temperature.<sup>21</sup> In 2010, Ogawa *et al.* indicated that the UV-assisted photogeneration of the MC form in solid phase strongly depends on the temperature.<sup>22</sup> He concluded that the photoisomerization is a common feature at low temperature but

<sup>a</sup>Institut Lavoisier de Versailles, UMR 8180, Université Paris-Saclay, Université de Versailles Saint-Quentin en Yvelines, 45 Avenue des Etats-Unis, 78035 Versailles cedex, France. E-mail: olivier.oms@uvsq.fr.

<sup>b</sup>Institut de Chimie Moléculaire et des Matériaux d'Orsay, Université Paris Sud, Université Paris-Saclay F-91405 Orsay, France.

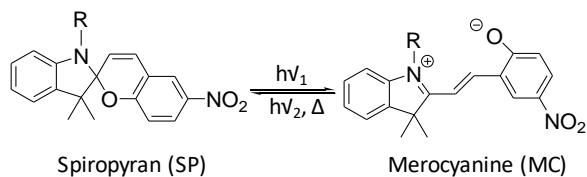
<sup>c</sup>Institut des Matériaux Jean Rouxel, Université de Nantes, CNRS, 2 rue de la Houssinière, BP 32229, 44322 Nantes cedex, France. E-mail: remi.dessapt@cnrs-imn.fr.

<sup>d</sup>Laboratoire d'Electrochimie et de Chimie Physique du Corps Solide, Institut de Chimie (UMR 7177 CNRS), Université de Strasbourg, 4 rue Blaise Pascal, 67081 Strasbourg Cedex, France. E-mail: lruhlmann@unistra.fr

<sup>‡</sup> These authors contribute equally to this work.

ESI† Footnotes relating to the title and/or authors should appear here.

Electronic Supplementary Information (ESI) available: [details of any supplementary information available should be included here]. See DOI: 10.1039/x0xx00000x



**Scheme 1** Photoinduced equilibrium involving a spiropyran derivative

rather rare under ambient conditions. Besides, some of us have developed an original class of hybrid compounds photoactive at room temperature in the solid state. These species associate polyoxometalates (POMs) and spiropyrans. POMs, which can be described as discrete anionic metal-oxide clusters, have been widely studied for their catalytic properties,<sup>23</sup> but their rich optical properties have also been deeply reported.<sup>24</sup> Thus, ionic assemblies were first isolated starting from a cationic spiropyran and various polyoxomolybdates.<sup>25</sup> This study highlighted the crucial role of the nature of the POM unit onto the initial color of the hybrids and the efficiency of the photoisomerization process. While a strong overlap between the SP and POM absorption bands in the 300-400 nm range together with charge transfers between the SP entity and the POM can strongly alter the optical properties of such hybrids, the polarity of the POM counter-ion can drastically enhance the rate of the SP→MC conversion.<sup>26</sup> Besides, covalent assemblies have also been investigated leading to the synthesis of the unsymmetrical  $(\text{TBA})_3[\text{MnMo}_6\text{O}_{18}\{(\text{OCH}_2)_3\text{CNH}_2\}\{(\text{OCH}_2)_3\text{CNHCO}(\text{C}_{20}\text{H}_{19}\text{N}_2\text{O}_3)\}]$  hybrid POM (noted as  $(\text{TBA})_3[\text{MnMo}_6\text{-SP}]$ ) (TBA = tetrabutylammonium cations) by reacting the well-known amino-functionalized Mn-Anderson type POM  $(\text{TBA})_3[\text{MnMo}_6\text{O}_{18}\{(\text{OCH}_2)_3\text{CNH}_2\}_2]$  with a spiropyran carboxylic acid SPCOOH *via* a peptide coupling reaction.<sup>27</sup> The resulting free amino group in one face of the crown-shaped inorganic platform allowed a post-functionalization step which led to the elaboration of a fluorescent photoswitch<sup>28</sup> or amphiphilic hybrid POMs.<sup>29</sup> A biphotochromic compound has also been isolated by the covalent grafting of a spironaphthoxazine (SN) moiety which is also a UV-activated photochrome. In contrast with the purple merocyanine form obtained after irradiation from spiropyran derivatives, the photoisomerization of the symmetrical Mn-Anderson type POM functionalized with two SN groups lead to a blue powder, extending the palette of accessible colors.<sup>30</sup>

Besides the photochromic properties of spiropyrans, it has been evidenced that the photogenerated merocyanine dyes can present highly interesting luminescent properties.<sup>10</sup> However, it is only recently that the luminescence of a POM/merocyanine hybrid has been investigated in solution,<sup>31</sup> and, to the best of our knowledge, neither the solid-state luminescent properties nor the influence of the nature of the POM unit on the fluorescence of such dyes have been studied to date.

Herein, we report on the first Dawson-type POM functionalized with a spiropyran group  $(\text{TBA})_5[\text{P}_2\text{W}_{15}\text{V}_3\text{O}_{59}\{(\text{OCH}_2)_2\text{C}(\text{Et})\text{NHCO}(\text{C}_{20}\text{H}_{19}\text{N}_2\text{O}_3)\}]$  (noted as  $(\text{TBA})_5[\text{P}_2\text{W}_{15}\text{V}_3\text{-SP}]$ ) obtained from the precursor  $\text{SP}(\text{OH})_2$ . In addition, we also present the synthesis of the new hybrids  $(\text{TBA})_3[\text{AlMo}_6(\text{OH})_3\{(\text{OCH}_2)_3\text{CNHCO}(\text{C}_{20}\text{H}_{19}\text{N}_2\text{O}_3)\}]$  (noted as  $(\text{TBA})_3[\text{AlMo}_6\text{-SP}]$ ) and  $(\text{TBA})_3[\text{AlMo}_6(\text{OH})_3\{(\text{OCH}_2)_3\text{CNHCO}(\text{C}_{21}\text{H}_{19}\text{N}_2\text{O})\}]$  (noted as

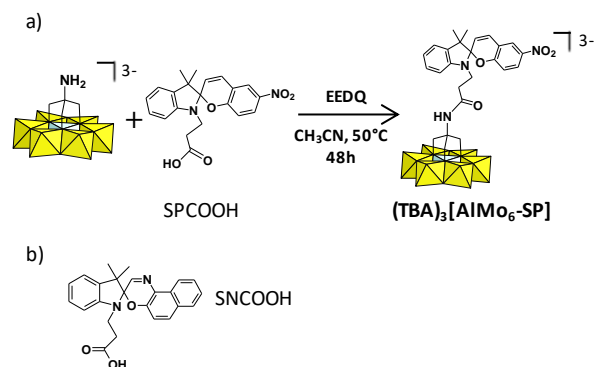


**Fig. 1** a) Schematic synthetic procedure leading to  $(\text{TBA})_3[\text{AlMo}_6\text{-SP}]$ . The TBA cations are not represented. Yellow octahedra {MoO<sub>6</sub>}; light blue octahedra {AlO<sub>6</sub>}; b) The spironaphthoxazine derivative SNCOOH

$(\text{TBA})_3[\text{AlMo}_6\text{-SN}]$ ) in which a spiropyran or a spironaphthoxazine entity, respectively, is covalently linked to an inorganic POM platform. The Al-Anderson type POM has been chosen for its large transparency window in the near UV and visible domains, contrary to the colored manganese(III) derivative previously considered for the elaboration of related systems.<sup>27</sup> An in-depth spectroelectrochemical study of these species has been achieved allowing to propose a mechanism of their different electrochemical processes. Importantly, along with the photochromic properties, the solid-state fluorescence of the photo-generated merocyanines connected to POMs has been investigated for the first time, allowing unambiguously demonstrating that the fluorescence of the organic fragment is strongly dependent on the nature of the anchoring inorganic platform.

## Results and discussion

### Synthesis of the hybrid materials

The synthesis of the hybrid Al-Anderson type POM  $(\text{TBA})_3[\text{AlMo}_6\text{-SP}]$  was achieved *via* a peptide coupling reaction between the unsymmetrical  $(\text{TBA})_3[\text{AlMo}_6(\text{OH})_3\{(\text{OCH}_2)_3\text{CNH}_2\}]$  POM and SPCOOH<sup>33</sup> (Fig. 1a). In this reaction, similar to that employed for the synthesis of the symmetric Mn-Anderson derivative, EEDQ (N-Ethoxycarbonyl-2-ethoxy-1,2-dihydroquinoline) was used as a coupling agent. The reaction was performed in refluxing acetonitrile with an excess of carboxylic acid. The targeted product is obtained after a first precipitation in a large volume of diethyl ether and purified after two new dissolution/precipitation cycles. Unfortunately, despite numerous attempts, we have not been able to obtain single crystals suitable for X-Ray diffraction studies. However, it has been fully characterized by means of complementary techniques. First, <sup>1</sup>H NMR spectroscopy demonstrates the presence of the spiropyran moiety and the integration values reveal a TBA/SP ratio of 3 that matches perfectly with the expected formulae (for example,  $\delta = 0.98$  ppm for the methyl groups of the TBA ions while well separated signals belonging to the aromatic part of the spiropyran are observed in the 6.6-8.1 ppm range, Fig. S1, ESI<sup>†</sup>). Secondly, in the <sup>13</sup>C NMR spectrum, the signal at 171.6 ppm corresponds to the amide function linking the two components (Fig. S2, ESI<sup>†</sup>). Thirdly, the  $\nu(\text{CO})$  stretching band of this specific function is observed in the IR

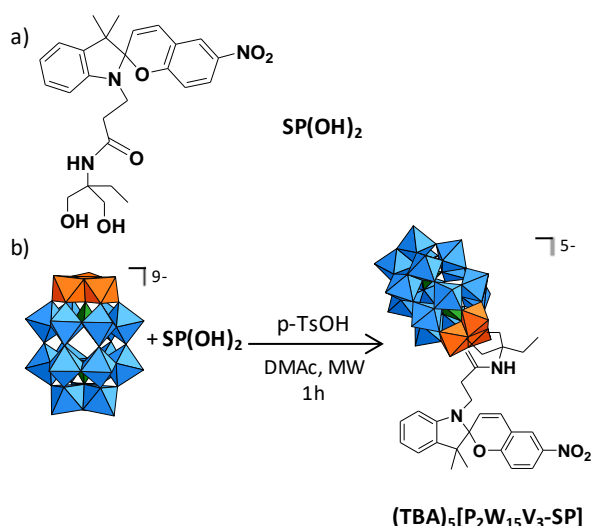


**Fig. 2** a) The spiropyran derivative **SP(OH)<sub>2</sub>**; b) Schematic synthetic pathway leading to **(TBA)<sub>5</sub>[P<sub>2</sub>W<sub>15</sub>V<sub>3</sub>-SP]**. Blue octahedra {WO<sub>6</sub>}; orange octahedra {VO<sub>6</sub>}.

spectrum at 1674 cm<sup>-1</sup> (Fig. S3, ESI<sup>+</sup>) whereas this signal appears at 1702 cm<sup>-1</sup> for the SPCOOH precursor. In addition, the integrity of the {AlMo<sub>6</sub>} platform is also ascertained by the terminal Mo=O vibration bands at 942, 920 and 900 cm<sup>-1</sup> along with the bridging Mo-O-Mo at 663 cm<sup>-1</sup>. Fourthly, the product is also characterized by a single peak in the <sup>27</sup>Al NMR spectrum at 16.34 ppm (Fig. S4, ESI<sup>+</sup>). Lastly, MALDI-TOF mass spectrometry was performed. This specific technique has already been successfully used for POM derivatives.<sup>34</sup> In the spectrum obtained in negative ion mode, the envelopes corresponding to monoanionic (such as [P+2Na+H<sub>2</sub>O]<sup>-</sup> at m/z = 1485.07) or dianionic (such as [P+TBA+DCTB]<sup>2-</sup> at m/z = 955.96) adducts can be given as examples of all the identified signals (P refers to [AlMo<sub>6</sub>(OH)<sub>3</sub>{(OCH<sub>2</sub>)<sub>3</sub>CNHCOC(C<sub>20</sub>H<sub>19</sub>N<sub>2</sub>O<sub>3</sub>)}]<sup>3-</sup> and DCTB is the matrix molecule (*trans*-2-[3-(4-*tert*-butylphenyl)-2-methyl-2-propenylidene]malononitrile)) (Fig. S5, ESI<sup>+</sup>).

**(TBA)<sub>3</sub>[AlMo<sub>6</sub>-SN]** was prepared by the same synthetic procedure using SNCOOH<sup>35</sup> (Fig. 1b) instead of SPCOOH. The ν(CO) stretching band at 1676 cm<sup>-1</sup> in the infrared spectrum (Fig. S6, ESI<sup>+</sup>) and the peak at 171.4 ppm in the <sup>13</sup>C NMR spectrum (Fig. S7, ESI<sup>+</sup>) clearly demonstrate the grafting of the organic part onto the inorganic platform through amide bond formation. The TBA/SN ratio of 3 deduced from the <sup>1</sup>H NMR spectrum (for example, δ = 0.98 ppm for the methyl groups of the TBA ions while well separated signals belonging to the aromatic part of the spironaphthoxazine are observed in the 6.7-8.6 ppm range, Fig. S8, ESI<sup>+</sup>) and the elemental analysis confirm the formation of the product, also characterized by one peak at 15.12 ppm in the <sup>27</sup>Al NMR spectrum (Fig. S9, ESI<sup>+</sup>).

While Parac-Vogt *et al.* described very recently a new way to post-functionalize Dawson-type POMs,<sup>36</sup> the synthetic methods leading to organically modified Dawson species usually consist in reacting a triol functionalized organic fragment with the (TBA)<sub>5</sub>[H<sub>4</sub>P<sub>2</sub>W<sub>15</sub>V<sub>3</sub>O<sub>62</sub>] inorganic precursor in refluxing dimethylacetamide or acetonitrile during a few days.<sup>37</sup> Attempts to graft the photochromic entity *via* a spiropyran bearing a triol group<sup>26</sup> onto the Dawson POM following this experimental procedure failed, leading to a mixture of uncharacterized compounds. However, Hasenknopf described in

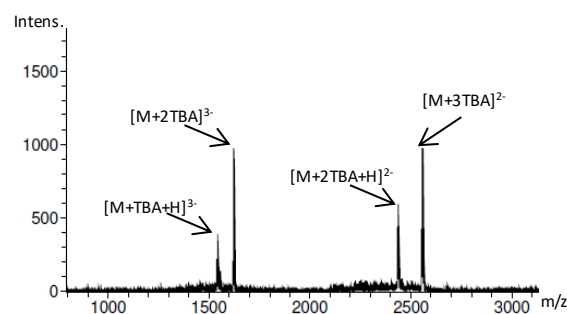


**Fig. 3** HR-ESI-MS spectrum (negative mode) of **(TBA)<sub>5</sub>[P<sub>2</sub>W<sub>15</sub>V<sub>3</sub>-SP]**. M refers to the anionic core [P<sub>2</sub>W<sub>15</sub>V<sub>3</sub>O<sub>59</sub>{(OCH<sub>2</sub>)<sub>2</sub>C(Et)NHCO(C<sub>20</sub>H<sub>19</sub>N<sub>2</sub>O<sub>3</sub>)}]<sup>5-</sup>.

2009 a synthetic pathway starting from a diol functionalized organic derivative and involving microwave radiations.<sup>38</sup> In an original way, not only the two oxygen atoms of the diol group but also the oxygen of the carbonyl function link the vanadium centres in the final product. In the aim to prepare **(TBA)<sub>5</sub>[P<sub>2</sub>W<sub>15</sub>V<sub>3</sub>-SP]** following this methodology, the synthesis of a spiropyran containing a diol group (noted **SP(OH)<sub>2</sub>**, Fig. 2a) has been successfully achieved by coupling SPCOOH with 2-amino-2-ethyl-1,3-propanediol. This new organic compound has been fully characterized through multinuclear NMR spectroscopies, mass spectrometry and elemental analysis (Fig. S10-S12, ESI<sup>+</sup>). And indeed, under microwave radiations and in the presence of a catalytic amount of para-toluenesulfonic acid (p-TsOH), the coupling reaction between (TBA)<sub>5</sub>[H<sub>4</sub>P<sub>2</sub>W<sub>15</sub>V<sub>3</sub>O<sub>62</sub>] and **SP(OH)<sub>2</sub>** in dimethylacetamide has proved to be highly effective, with a nearly quantitative yield in only one hour (Fig. 2b). Even if our numerous trials to get single crystals of **(TBA)<sub>5</sub>[P<sub>2</sub>W<sub>15</sub>V<sub>3</sub>-SP]** for X-ray diffraction analysis failed, the hybrid POM was also deeply characterized by a panel of complementary techniques (Fig. S13-S24, ESI<sup>+</sup>). Its <sup>31</sup>P NMR spectrum exhibits only two peaks at δ = -7.22 and -13.31 ppm related to the proximal and distal phosphorus atoms, respectively, evidencing the absence of Dawson-based byproduct (Fig. S13, ESI<sup>+</sup>). The <sup>1</sup>H NMR spectrum of **(TBA)<sub>5</sub>[P<sub>2</sub>W<sub>15</sub>V<sub>3</sub>-SP]** clearly demonstrates the presence of the photochromic group. Surprisingly and contrary to all the previously reported covalent SP/POM assemblies, signals related to the merocyanine isomer are clearly visible beside those of the closed spiro majority form (Fig. S14, ESI<sup>+</sup>). Moreover, an AB system centred at around δ = 5.4 ppm characterizes the protons of the two -CH<sub>2</sub>-O groups, confirming their covalent linkage to the inorganic part as alkoxide ligands.<sup>38</sup> In the <sup>13</sup>C NMR spectrum, we can note the signal of the C=O function at 188.7 ppm that is out of the range of typical amide function and characterizes its coordination to one vanadium centre (Fig. S15, ESI<sup>+</sup>). COSY, HSQC and HMBC 2D NMR studies have been performed (see the ESI for a detailed description of these experiments), allowing a complete attribution of the signals to the protons and carbon atoms belonging to the closed spiro form (Fig. S16-S18, ESI<sup>+</sup>). In addition, **(TBA)<sub>5</sub>[P<sub>2</sub>W<sub>15</sub>V<sub>3</sub>-SP]** has also been analyzed by electrospray ionization (HR-ESI-MS) in the negative ion mode. Strikingly, the unique four peaks of the spectrum are attributed to the [M+TBA+H]<sup>3-</sup> (m/z = 1546.7), [M+2TBA]<sup>3-</sup> (m/z = 1626.8), [M+2TBA+H]<sup>2-</sup> (m/z = 2440.7) and [M+3TBA]<sup>2-</sup> (m/z = 2561.4)

Compounds	SP or SN	Mn <sup>IV/III</sup>	V <sup>V/IV</sup>	Mn <sup>III</sup> /Mn <sup>II</sup>	-NO <sub>2</sub>	Mo <sup>VI/V</sup>	W <sup>VI/V</sup>
<b>SP(OH)<sub>2</sub><sup>a</sup></b>	1.062 <sup>irr</sup>	-	-	-	-1.158 (119)	-	-
<b>(TBA)<sub>3</sub>[AlMo<sub>6</sub>-SP]<sup>a</sup></b>	1.171 <sup>irr</sup>	-	-	-	-1.221 <sup>irrc</sup>	- <sup>c</sup>	-
<b>(TBA)<sub>3</sub>[AlMo<sub>6</sub>-SN]<sup>a</sup></b>	1.032 <sup>irr</sup>	-	-	-	-	- <sup>c</sup>	-
<b>(TBA)<sub>3</sub>[MnMo<sub>6</sub>-SP]<sup>a,b</sup></b>	1.061 <sup>irr</sup>	0.831 (222)	-	-0.541 (114)	-1.330 (133)	- <sup>c</sup>	-
<b>(TBA)<sub>5</sub>[P<sub>2</sub>W<sub>15</sub>V<sub>3</sub>-SP]<sup>a</sup></b>	1.066 <sup>irr</sup>	-	0.256 (220) -0.253 <sup>irr</sup> -0.597 (120)	-	-1.123 <sup>d</sup> (155)	-	-1.264 <sup>e</sup> (128)

<sup>a</sup> Potentials in V vs. SCE were obtained from cyclic voltammetry in CH<sub>3</sub>CN with 0.1 mol L<sup>-1</sup> TBAPF<sub>6</sub>. Scan rate = 100 mV s<sup>-1</sup>. Working electrode: Glassy Carbon electrode (GC), d = 3 mm. The given half-wave potentials are equal to E<sub>1/2</sub> = (E<sub>pa</sub> + E<sub>pc</sub>)/2. Under bracket: ΔE<sub>p</sub> = |E<sub>pa</sub> - E<sub>pc</sub>| (in mV).

<sup>b</sup> see reference 27.

<sup>c</sup> not measured

<sup>d</sup> the reduction may be associated to the reduction of the W<sup>VI</sup>.

<sup>e</sup> the reduction may be associated to the reduction of the nitro unit.

**Table 1.** Electrochemical data for SP(OH)<sub>2</sub>, (TBA)<sub>3</sub>[AlMo<sub>6</sub>-SP], (TBA)<sub>3</sub>[AlMo<sub>6</sub>-SN], (TBA)<sub>3</sub>[MnMo<sub>6</sub>-SP]<sup>27</sup> and (TBA)<sub>5</sub>[P<sub>2</sub>W<sub>15</sub>V<sub>3</sub>-SP].

anionic species where M refers to [P<sub>2</sub>W<sub>15</sub>V<sub>3</sub>O<sub>59</sub>{(OCH<sub>2</sub>)<sub>2</sub>C(Et)NHCO(C<sub>20</sub>H<sub>19</sub>N<sub>2</sub>O<sub>3</sub>)}]<sup>5-</sup> (Fig. 3 and Fig. S19-S23, ESI<sup>†</sup>). This unambiguously confirms the overall charge of the anionic part and therefore the coordination mode of the photochromic entity onto the Dawson type POM. Finally, the IR spectrum of (TBA)<sub>5</sub>[P<sub>2</sub>W<sub>15</sub>V<sub>3</sub>-SP] (Fig. S24, ESI<sup>†</sup>) is in full agreement with a retention of the {P<sub>2</sub>W<sub>15</sub>V<sub>3</sub>} Dawson unit during the synthetic process.

In addition, TGA measurements of the three hybrid POMs were also achieved under oxygen atmosphere in the 25–650 °C range. For each compound, the observed total weight loss is in full agreement with the expected value considering oxides formation (Fig. S25–S27, ESI<sup>†</sup>.)

### Electrochemical and Spectroelectrochemical properties

The cyclic voltammograms (CVs) of SP(OH)<sub>2</sub>, (TBA)<sub>3</sub>[AlMo<sub>6</sub>-SP], (TBA)<sub>3</sub>[AlMo<sub>6</sub>-SN] and (TBA)<sub>5</sub>[P<sub>2</sub>W<sub>15</sub>V<sub>3</sub>-SP] are illustrated in Fig. 4 and Fig. S28–S30, ESI<sup>†</sup>. The peak potentials and the separation between the anodic and the cathodic peaks of the redox processes ΔE<sub>p</sub> are gathered in Table 1. First, the CV of SP(OH)<sub>2</sub> exhibits one irreversible oxidation at 1.062 V vs. SCE, attributed to the formation of the radical cation SP<sup>•+</sup>(OH)<sub>2</sub>. On the reverse scan between 0.7 and 0.9 V, two broad overlapping reduction peaks are observed (peaks a and b in Fig. 4A and Fig. S28, ESI<sup>†</sup>). The irreversible one-electron oxidation involves the indoline nitrogen of the spiropyran entity, which induces the formation of a new species. Actually, because of a subsequent fast chemical reaction, the oxidized radical cation SP<sup>•+</sup>(OH)<sub>2</sub> dimerizes by aryl C-C coupling to form the symmetrical cation dimer (HO)<sub>2</sub>SP<sup>+</sup>=SP<sup>+</sup>(OH)<sub>2</sub> (Scheme S1, ESI<sup>†</sup>). Browne *et al.* already studied the mechanism of the irreversible oxidation of spiropyrans.<sup>39</sup> In a few words, they proposed that the oxidation proceeds *via* a sequence of electrochemical (E) and chemical (C) reaction steps resulting in a E<sub>1</sub>C<sub>1</sub>C<sub>2</sub>E<sub>2</sub>E<sub>3</sub> mechanism (E<sub>1</sub>: one electron oxidation giving SP<sup>•+</sup>; C<sub>1</sub>: dimerization of SP<sup>•+</sup> to form the protonated dimer HSP<sup>+</sup>-SPH<sup>+</sup>; C<sub>2</sub>: double deprotonation to form SP-SP; E<sub>2</sub>E<sub>3</sub>: two successive oxidations to form SP<sup>+</sup>-SP<sup>+</sup> which explain the apparition of the broad overlapping reduction peaks observed on the reverse scan). Here, the oxidation of the resulting dimer (HO)<sub>2</sub>SP-SP(OH)<sub>2</sub> is easier than that of the initial SP(OH)<sub>2</sub> because of the higher delocalization of the positive charges over the whole structure and is observed from the second cycle (Fig. S29, ESI<sup>†</sup>). It results a more stable radical cation (HO)<sub>2</sub>SP<sup>•+</sup>-SP(OH)<sub>2</sub> and dication dimer (HO)<sub>2</sub>SP<sup>+</sup>=SP<sup>+</sup>(OH)<sub>2</sub> which lower the oxidation potentials. In the cathodic domain, one reversible reduction at -1.158 V vs. SCE is also measured (Fig. 4A), and corresponds to the reduction of the nitro pendant group.

(TBA)<sub>3</sub>[AlMo<sub>6</sub>-SP] shows similar redox behavior than SP(OH)<sub>2</sub> with one irreversible wave measured at 1.171 V vs. SCE associated to

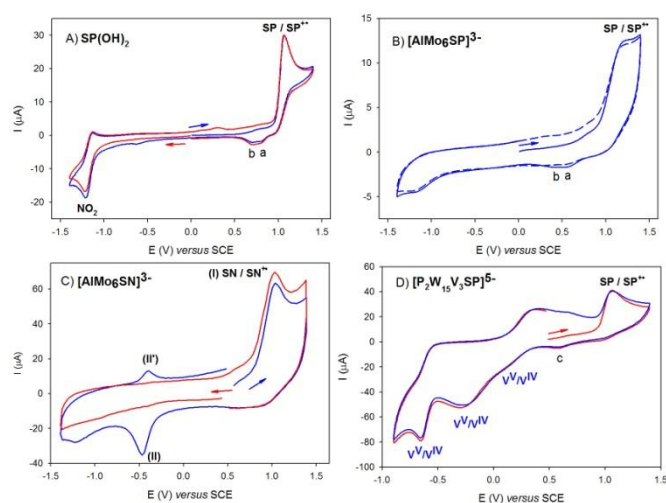


**Fig. 4** Cyclic voltammograms of A) SP(OH)<sub>2</sub>, B) (TBA)<sub>3</sub>[AlMo<sub>6</sub>-SP], C) (TBA)<sub>3</sub>[AlMo<sub>6</sub>-SN], and D) (TBA)<sub>5</sub>[P<sub>2</sub>W<sub>15</sub>V<sub>3</sub>-SP] (c = 1 mM) at a glassy carbon electrode (d = 3 mm) vs. SCE in CH<sub>3</sub>CN with 0.1 M TBAPF<sub>6</sub> as the supporting electrolyte. Scan rate: 100 mV s<sup>-1</sup>.

subsequent oxidation of the SP unit (Fig. 4B). Yet again, broad overlapping reduction peaks on the reverse sweep at 0.497 V and 0.586 V vs. SCE (peaks a and b) are detected indicating the formation of the dimer obtained by radical coupling reaction between two radical cations  $SP^{\bullet+}$ . The ill-defined wave detected near -1.2 V vs. SCE might be attributed to the reduction of the nitro unit.

In the case of  $(TBA)_3[AlMo_6-SN]$ , one irreversible oxidation of the SN unit is observed at 1.032 V vs. SCE, showing an oxidation potential close to that of the SP group in  $(TBA)_3[AlMo_6-SP]$  (Fig. 4C). Plot of the irreversible anodic current ( $I_{pa}$ ) vs the square root of the scan rate  $v^{1/2}$  (peak I) displays a linear dependence (Fig. S30, ESI<sup>†</sup>) showing that the current is limited by the diffusion of  $[AlMo_6-SN]^{3-}$  to the electrode surface as expected for a process involving species in solution. After the irreversible oxidation, one reversible signal appears at -0.429 V vs. SCE (peaks II and II'). Again, both peaks II and II' show similarly a linear dependence of the anodic and cathodic peak current versus the square root of the scan rate  $v^{1/2}$ .

In the case of  $(TBA)_5[P_2W_{15}V_3-SP]$ , the irreversible oxidation of the SP unit is still observed at 1.066 V vs. SCE. On the reverse scan, a broad reduction peak (peak c) appears at 0.596 V vs. SCE (Fig. 4D). Moreover, three mono-electronic successive waves corresponding to the successive reductions of the three V<sup>V</sup> centres are observed. The two redox processes measured at 0.256 V and -0.597 V vs. SCE are quasi-reversible while the reduction observed at -0.253 V vs. SCE is irreversible. Such redox processes concerning V<sup>V</sup> ions were already reported by Hill *et al.*<sup>40</sup> and some of us.<sup>37f,37g</sup> The reduction of the nitro unit for  $(TBA)_5[P_2W_{15}V_3-SP]$  is observed at -1.264 V vs. SCE after the reduction of the three V<sup>V</sup> centres (Fig. S31, ESI<sup>†</sup>).

Following the study of their electrochemical properties by CV, solution spectroelectrochemical studies were carried out to investigate the electronic properties of all the compounds (Fig. 5-7, Fig. S29 and Fig. S32-S35, ESI<sup>†</sup>).

The electrochemical oxidation of  $SP(OH)_2$  (Fig. 5 and Fig. S29, ESI<sup>†</sup>) induces strong changes in the UV-Vis-NIR absorption spectra. Actually, the initial UV-Vis-NIR absorption spectrum of the colorless solution of  $SP(OH)_2$  corresponds to the blue curve in Fig. 5A. Upon oxidation to the cation radical state  $SP^{\bullet+}(OH)_2$ , a decrease in the bands at 242 nm, 263 nm and 337 nm were observed with the appearance and concomitant increase of new bands at 260 nm, 298 nm (weak) and 514 nm (strong) indicating that the resulting compound becomes colored (green curve of Fig. 5A). The CV obtained onto the Pt grid electrode, during the UV-Vis-NIR spectroelectrochemical studies, still indicates that this process is irreversible. As previously described (radical coupling step followed by a double deprotonation in Scheme S1, ESI<sup>†</sup>), the dimer  $(HO)_2SP-SP(OH)_2$  is formed during this oxidation step. At this stage, because the spectroelectrochemical studies is carried out under continuous illumination using white light, reversible photoconversion of  $(HO)_2SP-SP(OH)_2$  to  $(HO)_2SP-MC(OH)_2$  and  $(HO)_2MC-MC(OH)_2$  can happen. Finally, the two further oxidation steps of the SP units of  $(HO)_2SP-SP(OH)_2$  lead to the formation of  $(HO)_2SP^+=SP(OH)_2$ . Thus the UV-Vis-NIR absorption spectrum could illustrate the formation of a mixture of  $(HO)_2SP-MC(OH)_2$ ,  $(HO)_2MC-MC(OH)_2$  and  $(HO)_2SP^+=SP(OH)_2$  species. For the former compounds, higher delocalization of the positive charge over each MC unit (zwitterion

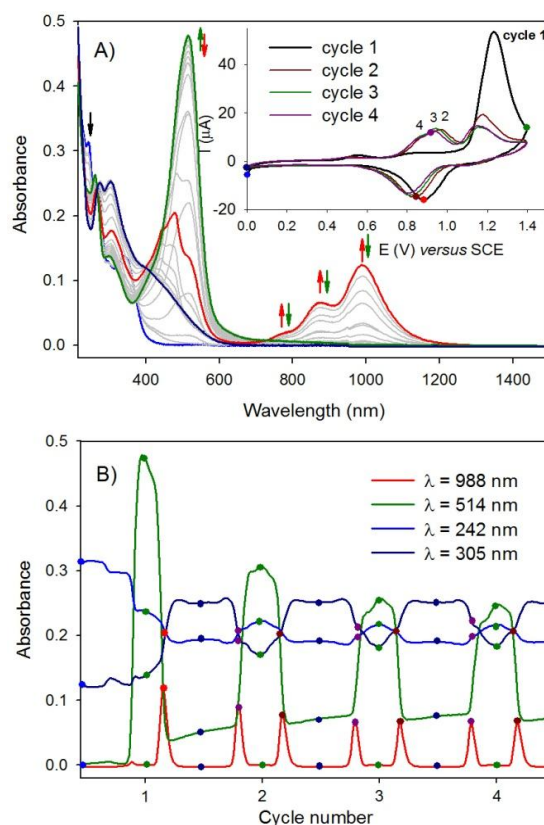


**Fig. 5** UV-Vis-NIR spectroelectrochemical study of  $SP(OH)_2$  ( $c = 1$  mM) at ambient temperature upon electrochemical oxidation in  $CH_3CN$  with 0.1 M TBAPF<sub>6</sub> as the supporting electrolyte recorded with an optically transparent thin-layer (0.2 mm) electrochemical (OTTLE) cell equipped with a Pt minigrad WE and CaF<sub>2</sub> optical windows. A) UV-Vis-NIR spectra recorded during the four successive oxidations of the  $SP(OH)_2$  (between -0.2 and +1.2 V). Inset shows the corresponding CVs at scan rate of 0.02 V.s<sup>-1</sup>. B) Evolution of the intensity of absorption of the UV-vis-NIR spectra of  $SP(OH)_2$  at 988 nm, 514 nm, 305 nm and 242 nm over four switching cycles upon electrochemical reduction in the potential region of the oxidation step. See text for details.

open form) could explain the presence of the band at 514 nm. On the reverse scan, the appearance of the broad overlapping reduction peaks is still observed using platinum grid working electrode. At this potential (around 0.6-0.8 V, red circle in the inset of Fig. 5A), new absorption bands at 774 nm (weak), 874 nm (medium) and 988 nm (strong) grow together with the disappearance of the absorption band at 514 nm and the decrease of the bands at 453 and 480 nm (red curve, Fig. 5A). The mono-electronic reduction of  $(HO)_2SP^+=SP(OH)_2$  leads to the formation  $(HO)_2SP^{\bullet+}-SP(OH)_2$  which probably coexists with  $(HO)_2SP^{\bullet+}-MC(OH)_2$  due to the possible  $SP \rightleftharpoons MC$  photoconversion. This induces an important red shift in the UV-Vis-NIR absorption spectrum.  $(HO)_2SP^{\bullet+}-SP(OH)_2$  exists only at potential near 0.6-0.8 V vs. SCE, but disappears below 0.6 V vs. SCE or above 0.8 V vs. SCE as shown in Fig. 5B (on the red curve, the absorption at  $\lambda = 988$  nm is only observed in the 0.6-0.8 V range as indicated by red circles). The dimer  $(HO)_2SP-SP(OH)_2$  is recovered after a second reduction process. In a second cycle, the CV shows a lower oxidation potential (around 0.7 V), corresponding to the re-oxidation to  $(HO)_2SP^{\bullet+}-SP(OH)_2$  in a quasi reversible process. The lower oxidation potential

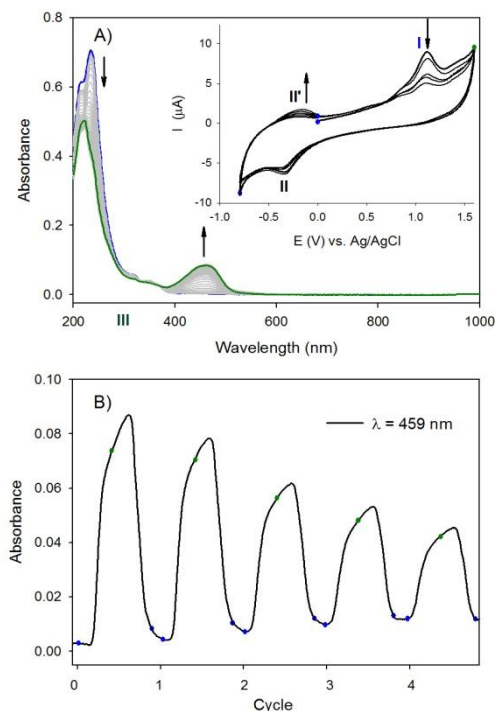


**Fig. 6** UV-Vis-NIR spectroelectrochemical study of  $(\text{TBA})_3[\text{AlMo}_6\text{-SN}]$  ( $c = 1 \text{ mM}$ ) at ambient temperature upon electrochemical oxidation in  $\text{CH}_3\text{CN}$  with  $0.1 \text{ M TBAPF}_6$  as the supporting electrolyte recorded with an optically transparent thin-layer (0.2 mm) electrochemical (OTTLE) cell equipped with an Pt minigrad WE and  $\text{CaF}_2$  optical windows. A) UV-Vis-NIR spectra recorded during five successive oxidations of  $(\text{TBA})_3[\text{AlMo}_6\text{-SN}]$  (between  $-0.7$  and  $+1.5 \text{ V}$ ). Inset shows the corresponding CVs at scan rate of  $0.02 \text{ V}\cdot\text{s}^{-1}$ . B) Evolution of the intensity of absorption of the UV-Vis-NIR spectra of  $(\text{TBA})_3[\text{AlMo}_6\text{-SN}]$  at  $459 \text{ nm}$  over five switching cycles upon electrochemical reduction in the potential region of the oxidation step.

vs the oxidation of the initial  $\text{SP}(\text{OH})_2$  is in line with a better delocalization of the positive charge(s).

For  $(\text{TBA})_3[\text{AlMo}_6\text{-SP}]$ , only little changes in the UV-Vis spectrum are observed during the oxidation step (Fig. S32A, ESI<sup>†</sup>). However, despite the small absorbance evolutions, differential UV-Vis-NIR spectroelectrochemical experiments (Fig. S32B, ESI<sup>†</sup>) evidence a decrease of the band located at  $243 \text{ nm}$  during the irreversible oxidation. This can be attributed to adsorption phenomena at the Pt electrode. This is confirmed by a peak at ca.  $1.040 \text{ V}$  when using Pt grid electrode whereas it is not observed when a glassy carbon electrode is used (Fig. 4B).

The electrochemical oxidation of  $(\text{TBA})_3[\text{AlMo}_6\text{-SN}]$  induces stronger changes in the UV-Vis-NIR absorption spectra than for  $(\text{TBA})_3[\text{AlMo}_6\text{-SP}]$  (Fig. 6 and Fig. S33-S34, ESI<sup>†</sup>). Upon oxidation of the starting colorless complex, a decrease in the absorption bands at  $210 \text{ nm}$  and  $239 \text{ nm}$  is observed with the appearance and concomitant increase of a new band at  $459 \text{ nm}$  (green curve of Fig. 6A). This absorption band disappears during the reverse scan until reaching reduction peak II (at  $-0.429 \text{ V}$ ). Furthermore, UV-Vis-NIR spectra recorded during five successive oxidations show a significant decrease of the intensity of the signal at  $459 \text{ nm}$  after the oxidation step with the number of iterative scans (Fig. 6B), evidencing instability during the formation of the radical cation  $\text{SN}^{\bullet+}$ . It must finally be noticed that the absorption bands in the

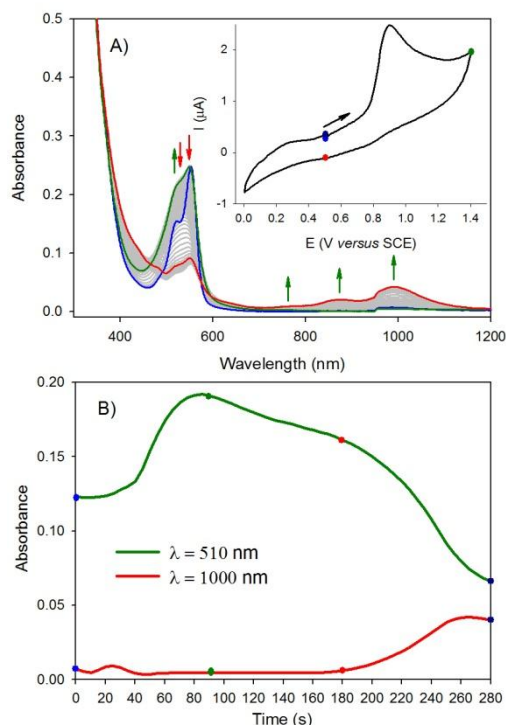


**Fig. 7** A) UV-Vis-NIR spectroelectrochemical study of  $(\text{TBA})_5[\text{P}_2\text{W}_{15}\text{V}_3\text{-SP}]$  ( $c = 1 \text{ mM}$ ) at ambient temperature upon electrochemical oxidation in  $\text{CH}_3\text{CN}$  with  $0.1 \text{ M TBAPF}_6$  as the supporting electrolyte recorded with an optically transparent thin-layer (0.2 mm) electrochemical (OTTLE) cell equipped with an Pt minigrad WE and  $\text{CaF}_2$  optical windows. Inset shows the corresponding CV at scan rate of  $0.01 \text{ V}\cdot\text{s}^{-1}$ . B) Evolution of the intensity of absorption of the UV-Vis-NIR spectra at  $510 \text{ nm}$  and  $1000 \text{ nm}$  during the CV.

$700\text{-}1200 \text{ nm}$  range observed in the case of the spirocyan derivatives are not observed for  $(\text{TBA})_3[\text{AlMo}_6\text{-SN}]$ .

The color of the initial solution of  $(\text{TBA})_5[\text{P}_2\text{W}_{15}\text{V}_3\text{-SP}]$  was pink-red confirming the presence of a certain amount of the  $[\text{P}_2\text{W}_{15}\text{V}_3\text{-MC}]^{5-}$  merocyanine form as observed by  $^1\text{H}$  NMR spectroscopy (see above). In agreement, the initial optical spectrum exhibits two bands at  $519 \text{ nm}$  and  $553 \text{ nm}$ . It can be proposed that the zwitterionic merocyanine isomer is stabilized by the formation of an ion pair between the polyanion and the positive charge of the organic fragment (Fig. 7 and Fig. S35, ESI<sup>†</sup>). Upon oxidation at  $1.066 \text{ V vs SCE}$  (green curve, Fig. 7), an increase in the absorption band at  $519 \text{ nm}$  was observed. It must be noted that the CV do not show a clear appearance of the broad overlapping reduction peaks observed on the reverse scan at  $0.596 \text{ V vs SCE}$  when a glassy carbon electrode is used. However, at a potential below  $0.600 \text{ V}$ , new absorption bands at  $783 \text{ nm}$  (weak),  $874 \text{ nm}$  (medium) and  $993 \text{ nm}$  (strong) grow together with the decrease of the absorption bands at  $519 \text{ nm}$  and  $553 \text{ nm}$  (red curve, Fig. 7B). Such behavior is similar to the parent compound  $\text{SP}(\text{OH})_2$  indicating the formation of the oxidized dimer. As already described for  $\text{SP}(\text{OH})_2$ , due to the continuous illumination using white light,  $\text{SP} \rightleftharpoons \text{MC}$  photoconversion may also happen. Importantly, the process is irreversible in this case as shown in Fig. 7B (green curve), indicating that, in contrast with the  $\text{SP}(\text{OH})_2$  parent compound, the formed species is highly stable in solution. This could be due to strong electrostatic interactions between the positively charged



Table 2 Photochromic kinetic parameters at room temperature of (TBA)<sub>3</sub>[AlMo<sub>6</sub>-SP], (TBA)<sub>3</sub>[AlMo<sub>6</sub>-SN] and (TBA)<sub>3</sub>[MnMo<sub>6</sub>-SP].

Photocoloration process							
Compound	A <sub>1</sub> <sup>a</sup>	A <sub>2</sub> <sup>a</sup>	k <sub>1</sub> <sup>c</sup> × 10 <sup>3</sup> (s <sup>-1</sup> ) <sup>b</sup>	k <sub>2</sub> <sup>c</sup> × 10 <sup>3</sup> (s <sup>-1</sup> ) <sup>b</sup>	t <sub>1/2</sub> <sup>c</sup> (min) <sup>c</sup>	R <sup>2</sup> <sup>d</sup>	
(TBA) <sub>3</sub> [AlMo <sub>6</sub> -SN]	0.743	0.782	11.3	2.3	2.1	0.9958	
(TBA) <sub>3</sub> [AlMo <sub>6</sub> -SP]	0.812	0.652	50.4	7.9	0.45	0.9983	
(TBA) <sub>3</sub> [MnMo <sub>6</sub> -SP]	0.697	1.114	49.9	9.1	0.65	0.9983	
Thermal fading process in the dark							
Compound	A <sub>0</sub> <sup>a</sup>	A <sub>1</sub> <sup>a</sup>	A <sub>2</sub> <sup>a</sup>	k <sub>1</sub> <sup>f</sup> × 10 <sup>3</sup> (s <sup>-1</sup> ) <sup>b</sup>	k <sub>2</sub> <sup>f</sup> × 10 <sup>3</sup> (s <sup>-1</sup> ) <sup>b</sup>	t <sub>1/2</sub> <sup>f</sup> (min) <sup>c</sup>	R <sup>2</sup> <sup>d</sup>
(TBA) <sub>3</sub> [AlMo <sub>6</sub> -SN]	1.199	0.483	0.165	0.2	3.6	28.1	0.9986
(TBA) <sub>3</sub> [AlMo <sub>6</sub> -SP]	1.266	0.040	0.010	0.1	7.6	52.2	0.9978
(TBA) <sub>3</sub> [MnMo <sub>6</sub> -SP]	1.730	0.048	0	0.4	0	31.4	0.9655
Fading process under visible-light irradiation <sup>e</sup>							
Compound	A <sub>0</sub> <sup>a</sup>	A <sub>1</sub> <sup>a</sup>	A <sub>2</sub> <sup>a</sup>	k <sub>1</sub> <sup>f</sup> × 10 <sup>3</sup> (s <sup>-1</sup> ) <sup>b</sup>	k <sub>2</sub> <sup>f</sup> × 10 <sup>3</sup> (s <sup>-1</sup> ) <sup>b</sup>	t <sub>1/2</sub> <sup>f</sup> (min) <sup>c</sup>	R <sup>2</sup> <sup>d</sup>
(TBA) <sub>3</sub> [AlMo <sub>6</sub> -SN]	1.474	0.707	0.542	0.5	25.6	4.3	0.9925
(TBA) <sub>3</sub> [AlMo <sub>6</sub> -SP]	1.374	0.938	0.078	0.1	3.7	89.5	0.9995
(TBA) <sub>3</sub> [MnMo <sub>6</sub> -SP]	1.851	1.398	0.045	0.2	42.2	73.3	0.9998

<sup>a</sup>The Abs<sup>λ<sub>max</sub></sup>(t) vs t plots were fitted as Abs<sup>λ<sub>max</sub></sup>(t) = (A<sub>1</sub>+A<sub>2</sub>) - A<sub>1</sub>exp(-k<sub>1</sub><sup>c</sup>t) - A<sub>2</sub>exp(-k<sub>2</sub><sup>c</sup>t) for the coloration process and as Abs<sup>λ<sub>max</sub></sup>(t) = (A<sub>0</sub>-A<sub>1</sub>-A<sub>2</sub>) + A<sub>1</sub>exp(-k<sub>1</sub><sup>f</sup>t) + A<sub>2</sub>exp(-k<sub>2</sub><sup>f</sup>t) for the fading ones. <sup>b</sup>Coloration (k<sup>c</sup>) and fading (k<sup>f</sup>) rate constants. <sup>c</sup>For the coloration process, the half-life time t<sub>1/2</sub><sup>c</sup> is defined as the UV irradiation time required for Abs<sup>λ<sub>max</sub></sup>(t) to reach half of its maximum value. For the fading ones, t<sub>1/2</sub><sup>f</sup> is defined as the irradiation time required for Abs<sup>λ<sub>max</sub></sup>(t) to reach the A<sub>0</sub>-(A<sub>1</sub>+A<sub>2</sub>)/2 value. <sup>d</sup>Regression coefficient for the Abs<sup>λ<sub>max</sub></sup>(t) vs t plot. <sup>e</sup>λ<sub>ex</sub> = 590 nm for (TBA)<sub>3</sub>[AlMo<sub>6</sub>-SP] and (TBA)<sub>3</sub>[MnMo<sub>6</sub>-SP]; λ<sub>ex</sub> = 630 nm for (TBA)<sub>3</sub>[AlMo<sub>6</sub>-SN].

appearance of two bands at λ<sub>max</sub> = 570 nm and 420 nm for (TBA)<sub>3</sub>[AlMo<sub>6</sub>-SP], and at 620 nm and 440 nm for (TBA)<sub>3</sub>[AlMo<sub>6</sub>-SN], which are characteristic of the MC forms.<sup>27,28,30</sup>

The bleaching processes occur at different rates by exposing the colored samples upon visible light or by keeping samples in darkness. In strong contrast, the red-purple powder of (TBA)<sub>3</sub>[P<sub>2</sub>W<sub>15</sub>V<sub>3</sub>-SP] does not exhibit photochromism under similar UV exposure. Besides, the sample cannot be bleached even by heating or after visible-light excitation for periods as long as a day. We may assume that the blocking of the SP ⇌ MC photoisomerization process could be attributed to the unusual linkage mode of the spiropyran to the POM platform via an amide function, that reinforces the interaction between both components, along with the high negative charge of the Dawson-type POM, which initially favors the ring opening process of the spiropyran group and stabilizes the zwitterionic merocyanine form, preventing photoswitching.

The coloration and fading kinetics of (TBA)<sub>3</sub>[AlMo<sub>6</sub>-SP], (TBA)<sub>3</sub>[AlMo<sub>6</sub>-SN] and (TBA)<sub>3</sub>[MnMo<sub>6</sub>-SP] measured under air and at room temperature have been fully investigated. The coloration kinetics have been quantified by monitoring the photogenerated absorption at λ<sub>max</sub> = 570 nm for (TBA)<sub>3</sub>[AlMo<sub>6</sub>-

SP], λ<sub>max</sub> = 580 nm for (TBA)<sub>3</sub>[MnMo<sub>6</sub>-SP], and at λ<sub>max</sub> = 620 nm for (TBA)<sub>3</sub>[AlMo<sub>6</sub>-SN] as a function of the UV irradiation time t, and the kinetics parameters are gathered in Table 2. The Abs<sup>λ<sub>max</sub></sup>(t) vs t plots have been adequately fitted using a biexponential rate law.<sup>27,28,30</sup> The photocoloration rates of the compounds can be well compared by considering their coloration half-life time (t<sub>1/2</sub><sup>c</sup>), namely the UV irradiation time required for Abs<sup>λ<sub>max</sub></sup>(t) to reach half of its maximum value. The fading kinetics of the samples have been also investigated to evaluate the efficiency of the MC → SP and MC → SN back conversions. The color fading rates have been measured in the dark (thermal fading) and under visible light at λ<sub>irr</sub> = 630 nm for (TBA)<sub>3</sub>[AlMo<sub>6</sub>-SN] (Fig. S39, ESI<sup>+</sup>), and at λ<sub>irr</sub> = 590 nm for (TBA)<sub>3</sub>[AlMo<sub>6</sub>-SP] (Fig. S40, ESI<sup>+</sup>) and (TBA)<sub>3</sub>[MnMo<sub>6</sub>-SP] (Fig. S41, ESI<sup>+</sup>), by monitoring the temporal decay of the photogenerated absorption bands of samples once irradiated under UV excitation. Decays were fitted using a biexponential rate law, and the fading kinetic parameters are detailed in Table 2. The fading rates of the compounds have been compared by considering their fading half-life time (t<sub>1/2</sub><sup>f</sup>). As shown in Fig. 8, (TBA)<sub>3</sub>[AlMo<sub>6</sub>-SP] and (TBA)<sub>3</sub>[AlMo<sub>6</sub>-SN] exhibit very fast photocoloration processes with t<sub>1/2</sub><sup>c</sup> values of 0.45 and 2.1 min respectively which evidences that the

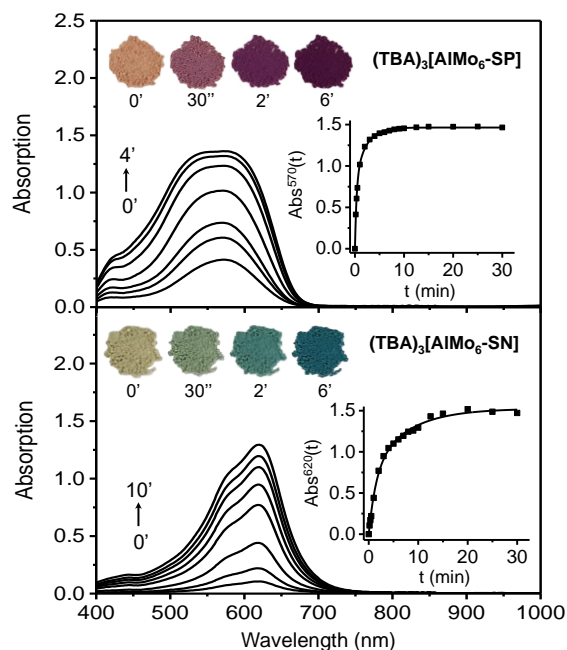


**Fig. 8** Photochromic properties and evolution of the photogenerated absorption at room temperature under UV irradiation ( $\lambda_{\text{irr}} = 365$  nm) after 0, 0.166, 0.333, 0.5, 1, 2, 3 and 4 min for  $(\text{TBA})_3[\text{AlMo}_6\text{-SP}]$ , and after 0, 0.166, 0.5, 1, 2, 3, 5, 7 and 10 min for  $(\text{TBA})_3[\text{AlMo}_6\text{-SN}]$ . Insets: Temporal evolutions of  $\text{Abs}^{\lambda^{\text{max}}}(t)$  under 365 nm-UV irradiation. Black lines show the fits of the  $\text{Abs}^{\lambda^{\text{max}}}(t)$  vs  $t$  plots according to the rate law  $\text{Abs}^{\lambda^{\text{max}}}(t) = (A_1 + A_2) - A_1 \exp(-k_1^c t) - A_2 \exp(-k_2^c t)$ .

photoisomerization of the spiro molecules are well efficient in the crystalline state. The coloration rate of  $(\text{TBA})_3[\text{AlMo}_6\text{-SP}]$  is quite comparable with that of  $(\text{TBA})_3[\text{MnMo}_6\text{-SP}]$  ( $t_{1/2}^c = 0.65$  min) (Fig. S42, ESI<sup>†</sup>) revealing that despite the fact that the Al-Anderson POM core exhibits a larger transparency window in the near UV and visible domains than its Mn counterpart (see above), it has no significant influence on the efficiency of the ring-opening process of the SP group.

Under visible-light irradiation, the MC  $\rightarrow$  SP back conversion occurs slowly for  $(\text{TBA})_3[\text{AlMo}_6\text{-SP}]$  ( $t_{1/2}^f = 89.5$  min) and  $(\text{TBA})_3[\text{MnMo}_6\text{-SP}]$  ( $t_{1/2}^f = 73.3$  min). Their thermal fading processes are also very limited, and the absorption loss after 4 hours is only 4 and 3% for  $(\text{TBA})_3[\text{AlMo}_6\text{-SP}]$  and  $(\text{TBA})_3[\text{MnMo}_6\text{-SP}]$ , respectively. This clearly indicates that in both cases the photoinduced zwitterionic MC form is well stabilized in the polar hybrid POM frameworks.<sup>27</sup> In marked contrast,  $(\text{TBA})_3[\text{AlMo}_6\text{-SN}]$  is a more efficient reversible photochromic system. Under visible-light excitation, it exhibits a fast and pronounced bleaching ( $t_{1/2}^f = 4.3$  min), with a significant absorption loss of 85% after 4 hours. The thermal fading process is more limited with an absorption loss of 53% after 4 hours. Finally, the robustness of  $(\text{TBA})_3[\text{AlMo}_6\text{-SN}]$  for repeatable “recording-erasing” processes was investigated at room temperature by monitoring the evolution of  $\text{Abs}^{620}$  of the powdered sample alternatively irradiated under UV light (365 nm) and visible light (630 nm) (Fig. S43, ESI<sup>†</sup>). The hybrid system shows a good cyclability over twenty five cycles.

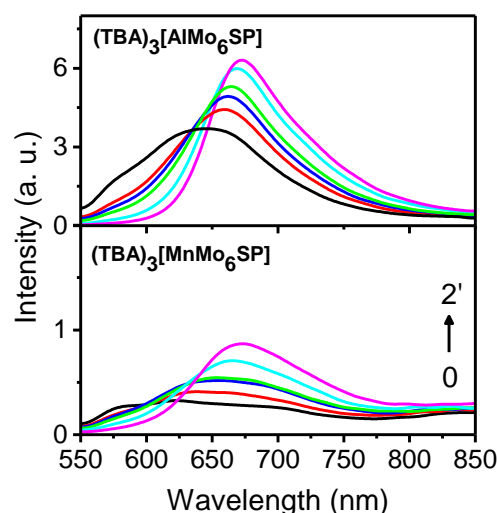


**Fig. 9** Evolution of the merocyanine luminescence (monitored at  $\lambda_{\text{exc}} = 500$  nm) under UV irradiation ( $\lambda_{\text{irr}} = 365$  nm) at room temperature after 0, 0.166, 0.333, 0.5, 1, and 2 min for  $(\text{TBA})_3[\text{AlMo}_6\text{-SP}]$  and  $(\text{TBA})_3[\text{MnMo}_6\text{-SP}]$ .

Besides its photochromic effect,  $(\text{TBA})_3[\text{AlMo}_6\text{-SP}]$  exhibits a brilliant photoswitchable red emission at room temperature when exposed to UV light at 365 nm. The emission intensity increases with the UV irradiation time (Fig. 9) and is maximum after 10 min i.e., when the photogenerated absorption band at 570 nm reaches its saturation level (Fig. 8). Hence, this emission can be assigned to the excited state of the MC form of the spiro pyran unit.<sup>41,42</sup> Indeed, for wavelengths up to 350 nm, the photoluminescence excitation (PLE) spectrum monitored at 675 nm (Fig. S44, ESI<sup>†</sup>) consists of two transitions which are very comparable to the absorption bands of the MC form. Thus the photoexcitation at 365 nm can be used to prompt the ring-opening process of the SP molecules, and the visible radiation at 500 nm can be used to monitor the luminescence properties. In spite of the initial bleaching of the powdered sample under visible light ( $\lambda_{\text{irr}} = 590$  nm) for three hours, a small amount of the MC form persists, and its emission spectrum is composed of a broad band centred at 640 nm with a shoulder around 570 nm. In the first two minutes of UV irradiation, the emission band intensity gradually increases with the amount of MC form, while the maximum wavelength at 640 nm is continuously red-shifted to reach 675 nm. This peculiar bathochromic effect could be due to the progressive formation of merocyanine aggregates in the solid state.<sup>43</sup> The luminescence properties have never been reported on the Mn-counterpart  $(\text{TBA})_3[\text{MnMo}_6\text{-SP}]$ .<sup>27</sup> Although its emission is not detectable with naked eyes at room temperature, an accurate investigation shows that  $(\text{TBA})_3[\text{MnMo}_6\text{-SP}]$  also exhibits a photoswitchable red emission but with a much weaker intensity than that of  $(\text{TBA})_3[\text{AlMo}_6\text{-SP}]$  (Fig. 9). The photomodulation of luminescence of both compounds is well reversible. Upon visible-light irradiation ( $\lambda_{\text{irr}} = 590$  nm), the red emission band gradually decreases in intensity with the irradiation time (Fig. S45, ESI<sup>†</sup>) associated to a progressive blue shift of the maximum emission wavelength. In contrast, no luminescence was monitored for the red-purple powder of  $(\text{TBA})_5[\text{P}_2\text{W}_{15}\text{V}_3\text{-SP}]$ ,

although it contains a significant amount of MC form (Fig. S36, ESI†).

The differences of emission efficiency between the three hybrid POMs can be tentatively explained considering possible luminescent quenching effects through a photoinduced electron transfer (PET) from the excited state of the merocyanine entity to the adjacent POM cores which are known to be good electron acceptors. Actually, the energy of the LMCT transitions of the POM units increases in the following order: **(TBA)<sub>5</sub>[P<sub>2</sub>W<sub>15</sub>V<sub>3</sub>-SP]** < **(TBA)<sub>3</sub>[MnMo<sub>6</sub>-SP]** < **(TBA)<sub>3</sub>[AlMo<sub>6</sub>-SP]** (Fig. S38, ESI†). This illustrates that the Dawson-type POM shows the highest electron affinity, and is easier to reduce than the Mn-Anderson and Al-Anderson type POMs, respectively. This is also in full agreement with the reduction potentials reported in Table 1:  $E_{1/2}$  ( $V^V/V^{IV}$ ) = 0.256 V for **(TBA)<sub>5</sub>[P<sub>2</sub>W<sub>15</sub>V<sub>3</sub>-SP]**,  $E_{1/2}$  (Mn<sup>III</sup>/Mn<sup>II</sup>) = -0.541 V for **(TBA)<sub>3</sub>[MnMo<sub>6</sub>-SP]** and the reduction of the Mo<sup>VI</sup> centers are not observed in the studied potential range for **(TBA)<sub>3</sub>[AlMo<sub>6</sub>-SP]**. Moreover, previous studies devoted to photoactive phospholium,<sup>44</sup> porphyrinic<sup>45</sup> or iridium(III)<sup>46,47</sup> hybrid POMs evidenced that luminescence quenching effects through a PET process increase with the electron acceptors abilities of the POMs, in direct line with what we experimentally observed herein.

## Conclusions

The synthesis of the two new covalent Al-Anderson type POM/spiromolecule hybrids **(TBA)<sub>3</sub>[AlMo<sub>6</sub>-SP]** and **(TBA)<sub>3</sub>[AlMo<sub>6</sub>-SN]** together with the first Dawson-type POM-spiropyran dyad **(TBA)<sub>5</sub>[P<sub>2</sub>W<sub>15</sub>V<sub>3</sub>-SP]** was successfully achieved. An in-depth investigation of the solution electrochemical and spectroelectrochemical properties evidences a dimerization process initiated during the oxidation of the indoline part for the spiropyran derivatives, leading to highly colored POM dimers. **(TBA)<sub>3</sub>[AlMo<sub>6</sub>-SP]** and **(TBA)<sub>3</sub>[AlMo<sub>6</sub>-SN]** also exhibit strong solid-state photochromism under UV-irradiation at room temperature. In particular, **(TBA)<sub>3</sub>[AlMo<sub>6</sub>-SN]** possesses high light-driven “recording–erasing” potentialities. In addition, compared to the previously reported **(TBA)<sub>3</sub>[MnMo<sub>6</sub>-SP]** system, the Al-Anderson POM core in **(TBA)<sub>3</sub>[AlMo<sub>6</sub>-SP]** has a high energy LMCT transitions, competing less with the spiropyran to absorb the excitation UV light. However, it does not significantly impact the efficiency of the photoisomerization process in **(TBA)<sub>3</sub>[AlMo<sub>6</sub>-SP]** and **(TBA)<sub>3</sub>[MnMo<sub>6</sub>-SP]** which exhibit comparable photoresponses. In marked contrast **(TBA)<sub>5</sub>[P<sub>2</sub>W<sub>15</sub>V<sub>3</sub>-SP]** is not photochromic under similar photoexcitation. Strikingly, this highly coloured compound initially contains a significant amount of the merocyanine isomer which has never been observed for other reported SP/POM hybrids. Both the specific linkage of the spiropyran to the Dawson-type platform and the high negative charge of the POM could prevent any efficient photoisomerization process. Importantly, this work also highlights for the first time the photoswitchable luminescence of covalent SP/POM dyads in the solid-state. The red emission which originates from the excited state of the photogenerated merocyanine is intense for **(TBA)<sub>3</sub>[AlMo<sub>6</sub>-SP]** and much more moderate for **(TBA)<sub>3</sub>[MnMo<sub>6</sub>-SP]**. Astonishingly, **(TBA)<sub>5</sub>[P<sub>2</sub>W<sub>15</sub>V<sub>3</sub>-SP]** is not luminescent despite the definite presence of the

merocyanine isomer. Both the optical and the electrochemical studies strongly suggest that the degree of emission quenching can be attributed to photoinduced electron transfer effects arising from the organic part to the inorganic component, which increase with the electron acceptor abilities of the POM. This work further underlines the essential role of the nature of the POM on the photophysical properties of the hybrid systems, and highlights that the Al-Anderson POM unit is a highly efficient inorganic platform to optimize both solid-state photochromic and photoluminescence properties.

## Experimental section

### Synthetic procedures

SPCOOH,<sup>33</sup> SNCOOH,<sup>35</sup> **(TBA)<sub>3</sub>[AlMo<sub>6</sub>(OH)<sub>3</sub>{(OCH<sub>2</sub>)<sub>3</sub>CNH<sub>2</sub>}]<sup>32</sup>** and **(TBA)<sub>5</sub>[H<sub>4</sub>P<sub>2</sub>W<sub>15</sub>V<sub>3</sub>O<sub>62</sub>]**<sup>48</sup> were synthesized following previously reported procedures.

### Synthesis of SP(OH)<sub>2</sub>

2-amino-2-ethyl-1,3-propanediol (0.115 g, 0.97 mmol) is added to a mixture of SP(OH)<sub>2</sub> (0.300 g, 0.79 mmol) and EEDQ (0.234 g, 0.95 mmol) in 5 mL of ethanol (EtOH). The resulting suspension is then heated to 50°C overnight. The dark red solution was cooled to room temperature and the solvent is evaporated under reduced pressure. The crude product (oily residue) was purified by silica gel chromatography column with a gradient dichloromethane (CH<sub>2</sub>Cl<sub>2</sub>)/ethyl acetate (AcOEt) co-solvent as eluent (from 8/2 to 3/7). **SP(OH)<sub>2</sub>** (0.193 g, 0.40 mmol) was isolated as a red powder with 50% yield.

<sup>1</sup>H NMR (CDCl<sub>3</sub>, 300K, 300 MHz) δ 8.00-8.06 (m, 2H, ArH), 7.20 (td, 1H, ArH, J = 7.6 Hz, J' = 1.3 Hz), 7.10 (dd, 1H, ArH, J = 7.2 Hz, J' = 1.0 Hz), 6.96-6.86 (m, 2H, ArH), 6.81-6.76 (m, 1H), 6.68 (d, 1H, J = 7.7 Hz), 5.98 (br, 1H, NH), 5.88 (d, 1H, J = 10.4 Hz), 3.81-3.44 (m, 8H, NCH<sub>2</sub> + C-(CH<sub>2</sub>OH)<sub>2</sub>), 2.66-2.35 (m, 2H, CH<sub>2</sub>-C(O)), 1.59 (q, 2H, C-CH<sub>2</sub>-CH<sub>3</sub>, J = 7.4 Hz), 1.27 (s, 3H, C-CH<sub>3</sub>), 1.15 (s, 3H, C-C-CH<sub>3</sub>), 0.80 (t, 3H, C-CH<sub>2</sub>-CH<sub>3</sub>, J = 7.4 Hz).

<sup>13</sup>C NMR (CDCl<sub>3</sub>, 300K, 75 MHz) δ 172.6, 159.4, 146.4, 141.2, 135.9, 128.5, 127.9, 126.0, 122.9, 122.0, 121.9, 120.0, 118.7, 115.5, 106.8, 65.6, 61.4, 53.0, 40.1, 37.0, 25.8, 25.6, 19.9, 14.2, 7.6.

Elemental analysis calcd for C<sub>26</sub>H<sub>31</sub>N<sub>3</sub>O<sub>6</sub>·0.5 AcOEt: C 63.93; H 6.66; N 7.99; found C 62.90; H 6.66; N 8.18.

### Synthesis of **(TBA)<sub>5</sub>[P<sub>2</sub>W<sub>15</sub>V<sub>3</sub>O<sub>59</sub>{(OCH<sub>2</sub>)<sub>2</sub>C(Et)NHCO(C<sub>20</sub>H<sub>19</sub>N<sub>2</sub>O<sub>3</sub>)]** (noted as **(TBA)<sub>5</sub>[P<sub>2</sub>W<sub>15</sub>V<sub>3</sub>-SP]**)

**(TBA)<sub>5</sub>[H<sub>4</sub>P<sub>2</sub>W<sub>15</sub>V<sub>3</sub>O<sub>62</sub>]** (100 mg, 19.3 μmol, 1 equiv.), pTsOH (2.2 mg, 0.6 equiv., 11.5 μmol) and **SP(OH)<sub>2</sub>** (13 mg, 24.6 μmol, 1.4 equiv.) were suspended in dry dimethylacetamide (0.4 mL). The mixture was heated under microwave to 80°C for 1 hour. The initial dark orange solution turned purple and was cooled to room temperature and poured onto diethylether (Et<sub>2</sub>O). The resulting solid was redissolved in acetonitrile (MeCN) and reprecipitated by addition of diethylether. Two other reprecipitation cycles (MeCN/EtOH and MeCN/Et<sub>2</sub>O) were carried out. The final purple solid was dried under vacuum, yielding **(TBA)<sub>5</sub>[P<sub>2</sub>W<sub>15</sub>V<sub>3</sub>-SP]·Et<sub>2</sub>O**. (m = 101 mg, 19 μmol, 98 %).

$^1\text{H}$  NMR ( $\text{CD}_3\text{CN}$ , 300K, 360 MHz)  $\delta$  9.55 (1H, s, NH); 8.07 (1H, d, J = 2.7 Hz, H3); 7.97 (1H, dd, J = 2.7 Hz, J' = 8.7 Hz, H4); 7.46 (1H, td, J = 7.6 Hz, J' = 1.0 Hz, H8); 7.19 (2H, s+t, J = 5.2 Hz, H1+H6); 7.09 (1H, d, J = 7.3 Hz, H9); 6.87 (1H, t, J = 7.3 Hz, H7); 6.76 (1H, d, J = 9 Hz, H5) 13 Hz; 6.07 (1H, d, J = 10.6 Hz, H2); 5.52 (2H, d, J = 13 Hz,  $\text{CH}_2\text{O}$ ), 5.29 (2H, d, J = 13 Hz,  $\text{CH}_2\text{O}$ ), 4.12 (2H, m,  $\text{CH}_2\text{N}$ ); 3.16 (40H, m, TBA  $\text{CH}_2$ ); 3.01 (2H, m,  $\text{CH}_2(\text{C}=\text{O})$ ); 1.74 (1H, m, Hi); 1.63 (40H, m, TBA  $\text{CH}_2$ ); 1.41 (40H, m, TBA  $\text{CH}_2$ ); 1.23 (3H, m, He); 1.13 (6H, m, He' + Hj); 0.98 (60H, m, TBA terminal  $\text{CH}_3$ ).

$^{13}\text{C}$  NMR ( $\text{CD}_3\text{CN}$ , 300K, 62.5 MHz)  $\delta$  188.70, 160.6, 146.7, 142.1, 136.5, 130.0, 129.8, 126.5, 123.8, 123.4, 122.5, 120.6, 120.5, 116.6, 109.2, 108.2, 89.6, 64.6, 54.5, 40.1, 36.2, 29.1, 27.1, 26.2.

$^{31}\text{P}$  NMR ( $\text{CD}_3\text{CN}$ , 300K, 250 MHz)  $\delta$  -7.22, -13.31.

Elemental analysis calcd. for  $(\text{C}_{16}\text{H}_{36}\text{N})_{3.4}[\text{H}_{1.6}\text{P}_2\text{W}_{15}\text{V}_3\text{O}_{59}(\text{SP}(\text{O})_2)]_3 \cdot \text{Et}_2\text{O}$ : C 19.14, H 3.10, N 1.69; Exp. C 19.12, H 3.17, N 1.67.

EDX measurements: V/W = 0.21

N.B.: the labels of the hydrogen atoms are given in the ESI.

### Synthesis of $(\text{TBA})_3[\text{AlMo}_6(\text{OH})_3\{(\text{OCH}_2)_3\text{CNHCO}(\text{C}_{20}\text{H}_{19}\text{N}_2\text{O}_3)\}]$ (noted as $(\text{TBA})_3[\text{AlMo}_6\text{-SP}]$ )

$(\text{TBA})_3[\text{AlMo}_6\text{O}_{18}(\text{OH})_3\{(\text{OCH}_2)_3\text{CNH}_2\}]$  (500 mg, 261  $\mu\text{mol}$ , 1 equiv.) was added to a suspension of SPCOOH (149 mg, 392  $\mu\text{mol}$ , 1.5 equiv.) and EEDQ (111 mg, 449  $\mu\text{mol}$ , 1.7 equiv.) in 20 mL of acetonitrile. The mixture was heated to 50°C for 4 days. The red solution was cooled to room temperature and the solvent was reduced to a minimum under vacuum. The concentrated solution was poured onto diethylether. The resulting solid was dissolved in a minimum of MeCN and reprecipitated by addition of diethylether. Three other MeCN/Et<sub>2</sub>O precipitation cycles were carried out. The final product was dried under vacuum, yielding  $(\text{TBA})_3[\text{AlMo}_6\text{-SP}]$  (551 mg, 256  $\mu\text{mol}$ , 98%) as a pink solid.

$^1\text{H}$  NMR ( $\text{CD}_3\text{CN}$ , 300 K, 300 MHz)  $\delta$  8.06 (1H, d, J = 2.6 Hz), 7.97 (1H, dd, J = 2.6 Hz, J' = 8.9 Hz), 7.14 (3H, m), 6.83 (1H, t, J = 7.3 Hz), 6.69 (1H, d, J = 8.9 Hz), 6.63 (1H, d, J = 7.8 Hz); 5.93 (1H, d, J = 10.4 Hz), 5.69 (1H, s, NH), 4.76 (6H, s,  $\text{CH}_2\text{O}$ ), 3.89 (3H, br, OH), 3.48 (1H, m,  $\text{CH}_2\text{N}$ ), 3.34 (1H, m,  $\text{CH}_2\text{N}$ ), 3.15 (24H, m, TBA  $\text{CH}_2$ ), 2.32 (2H, m,  $\text{CH}_2(\text{C}=\text{O})$ ), 1.64 (24H, m, TBA  $\text{CH}_2$ ), 1.38 (24H, m, TBA  $\text{CH}_2$ ), 1.23 (3H, s); 1.12 (3H, m), 0.98 (36H, m, TBA terminal  $\text{CH}_3$ ).

$^{13}\text{C}$  NMR ( $\text{CD}_3\text{CN}$ , 300 K, 75 MHz)  $\delta$  171.6, 160.3, 147.7, 142.1, 137.1, 129.3, 128.7, 126.5, 123.8, 123.0, 122.6, 120.3, 120.1, 116.3, 108.0, 107.9, 75.7, 59.2, 53.5, 41.1, 36.6, 26.3, 24.4, 20.4, 19.9, 13.9.

$^{27}\text{Al}$  NMR ( $\text{CD}_3\text{CN}$ , 300K, 78 MHz)  $\delta$  16.34.

FT-IR ( $\text{cm}^{-1}$ , ATR): 3420, 2962, 2935, 2874, 1674, 1609, 1576, 1516, 1483, 1460, 1381, 1335, 1275, 1159, 1129, 1087, 1030, 942, 920, 900, 806, 749, 663.

Elemental analysis calcd. for  $\text{AlMo}_6\text{O}_{28}\text{C}_{73}\text{H}_{137}\text{N}_6 \cdot 2\text{H}_2\text{O}$ : C 40.12; H 6.50; N 3.85; found C 40.70; H 6.29; N 3.93.

EDX measurements: Al/Mo = 0.17

### Synthesis of $(\text{TBA})_3[\text{AlMo}_6(\text{OH})_3\{(\text{OCH}_2)_3\text{CNHCO}(\text{C}_{21}\text{H}_{19}\text{N}_2\text{O})\}]$ (noted as $(\text{TBA})_3[\text{AlMo}_6\text{-SN}]$ )

$(\text{TBA})_3[\text{AlMo}_6\text{O}_{18}(\text{OH})_3\{(\text{OCH}_2)_3\text{CNH}_2\}]$  (500 mg, 261  $\mu\text{mol}$ , 1 equiv.) was added to a suspension of SNCOOH (151 mg, 391  $\mu\text{mol}$ , 1.5

equiv.) and EEDQ (111 mg, 449  $\mu\text{mol}$ , 1.7 equiv.) in 20 mL of acetonitrile. The mixture was heated to 50°C for 3 days. The green solution was cooled to room temperature and the solvent was reduced to a minimum under vacuum. The concentrated solution was poured onto diethylether. The resulting solid was dissolved in a minimum of acetonitrile and reprecipitated by addition of diethylether. Two other MeCN/Et<sub>2</sub>O precipitation cycles were carried out. The final product was dried under vacuum, yielding  $(\text{TBA})_3[\text{AlMo}_6\text{-SN}]$  (430 mg, 200  $\mu\text{mol}$ , 77%) as a pale green solid.

$^1\text{H}$  NMR ( $\text{CD}_3\text{CN}$ , 300 K, 300 MHz)  $\delta$  8.56 (1H, d, J = 8.3 Hz), 7.79 (3H, m), 7.61 (1H, t, J = 7.6 Hz), 7.43 (1H, t, J = 7.5 Hz), 7.20 (1H, t, J = 8.1 Hz), 7.10 (1H, d, J = 7.3 Hz), 6.99 (1H, m, J = 8.9 Hz), 6.87 (1H, t, J = 7.2 Hz), 6.72 (1H, d, J = 7.8 Hz), 5.70 (1H, s, NH), 4.75 (6H, s,  $\text{CH}_2\text{O}$ ), 3.51 (1H, m,  $\text{CH}_2\text{N}$ ), 3.33 (1H, m,  $\text{CH}_2\text{N}$ ), 3.13 (24H, m, TBA  $\text{CH}_2$ ), 2.45 (2H, m,  $\text{CH}_2(\text{C}=\text{O})$ ), 1.62 (24H, m, TBA  $\text{CH}_2$ ), 1.37 (24H, m, TBA  $\text{CH}_2$ ), 1.29 (3H, s), 1.27 (3H, s), 0.98 (36H, m, TBA terminal  $\text{CH}_3$ ).

$^{13}\text{C}$  NMR ( $\text{CD}_3\text{CN}$ , 300 K, 75 MHz)  $\delta$  171.4, 152.9, 147.7, 144.7, 136.7, 131.8, 131.1, 130.3, 128.9, 128.8, 128.1, 125.2, 123.7, 122.6, 122.5, 120.6, 117.9, 108.4, 100.4, 75.7, 59.2 ( $\text{C}_{\text{TBA}}$ ), 53.1, 41.49, 36.2, 25.7, 24.4 ( $\text{C}_{\text{TBA}}$ ), 20.8, 20.4 ( $\text{C}_{\text{TBA}}$ ), 13.9 ( $\text{C}_{\text{TBA}}$ ).

$^{27}\text{Al}$  NMR (78 MHz,  $\text{CD}_3\text{CN}$ )  $\delta$  (ppm) = 15.12.

IR (FTR):  $\nu$  ( $\text{cm}^{-1}$ ) = 2962 (s), 2936 (s), 2874 (s), 1676 (m), 1607 (w), 1561 (w), 1510 (w), 1484 (s), 1459 (s), 1382 (m), 1364 (m), 1308 (w), 1270 (w), 1248 (w), 1170 (w), 1132 (w), 1081 (m), 1032 (m), 942 (vs), 921 (vs), 904 (s), 819 (w), 754 (w), 663 (vs), 577 (w).

Elemental analysis calcd. for  $\text{C}_{76}\text{H}_{139}\text{AlMo}_6\text{N}_6\text{O}_{26} \cdot 4\text{H}_2\text{O}$ : C 40.97, H 6.63, N 3.77; found C 40.95; H 6.16; N 3.82.

EDX measurements: Al/Mo = 0.20

## Conflicts of interest

There are no conflicts to declare.

## Acknowledgements

This work was supported by CNRS, UVSQ, University Paris Sud, Université de Nantes, Université de Strasbourg, the French National Research Agency (ANR) as part of the "Investissements d'Avenir" program n°ANR-11-IDEX-0003-02 and CHARMMMAT ANR-11-LABX-0039, and the LUMOMAT project supported by the Région des Pays de la Loire. Susanna Volpe is gratefully acknowledged for her participation in the characterization of the photochromic properties.

## Notes and references

- a) X. Xie, G. Mistlberger and E. Bakker, *J. Am. Chem. Soc.*, 2012, **134**, 16929; b) T. A. Darwish, R. A. Evans, M. James and T. L. Hanley, *Chem. Eur. J.*, 2011, **17**, 11399; c) D. Kitagawa, K. Tanaka and S. Kobatake, *J. Mater. Chem. C*, 2017, **5**, 6210; d) M. Natali and S. Giordani, *Chem. Soc. Rev.*, 2012, **41**, 4010.
- a) C. C. Corredor, Z.-L. Huang, K. D. Belfield, A. R. Morales and M. V. Bondar, *Chem. Mater.*, 2007, **19**, 5165; b) M. H. Sharifian, A. R. Mahdavian and H. Salehi-Mobarakeh, *Langmuir*, 2017, **33**, 8023.

- 3 a) H. M. Menezes, Md. J. Islam, M. Takahashi and N. Tamaoki, *Org. Biomol. Chem.*, 2017, **15**, 8894; b) S. O. Poelma, S. S. Oh, S. Helmy, A. S. Knight, G. L. Burnett, H. T. Soh, C. J. Hawker and J. Read de Alaniz, *Chem Commun.*, 2016, **52**, 10525; c) M. Singer and A. Jäschke, *J. Am. Chem. Soc.*, 2010, **132**, 8372.
- 4 a) X. Chai, Y.X. Fu, T. D. James, J. Zhang, X.-P. He and H. Tian, *Chem. Commun.*, 2017, **53**, 9494; b) S. Chen, Z. Guo, S. Zhu, W.-E. Shi and W. Zhu, *ACS Appl. Mater. Interfaces*, 2013, **5**, 5623; c) A. Prasanna de Silva, *Chem. Asian J.*, 2011, **6**, 750.
- 5 a) F. Tong, D. Kitagawa, X. Dong, S. Kobatake and C. J. Bardeen, *Nanoscale*, 2018, **10**, 3393; b) N. Darwish, A. C. Aragones, T. Darwish, S. Ciampi and I. Diez-Perez, *Nano Lett.*, 2014, **14**, 7064.
- 6 R. Prado, M. Zayat and D. Levy, *Chem. Soc. Rev.*, 2011, **40**, 672.
- 7 H. M. Dhammika Bandara and S. C. Burdette, *Chem. Soc. Rev.*, 2012, **41**, 1809.
- 8 M. Irie, T. Fukaminato, K. Matsuda and S. Kobatake, *Chem. Rev.*, 2014, **114**, 12174.
- 9 Y. Yokoyama, *Chem. Rev.*, 2000, **100**, 1717.
- 10 a) R. Klajn, *Chem. Soc. Rev.*, 2014, **43**, 148; b) L. Kortekaas and W. R. Browne, *Chem. Soc. Rev.*, 2019, **48**, 3406.
- 11 a) L. Florea, A. McKeon, D. Diamond and F. Benito-Lopez, *Langmuir*, 2013, **29**, 2790; b) A. Abdollahi, Z. Alinejad and A. R. Mahdavian, *J. Mater. Chem. C*, 2017, **5**, 6588.
- 12 a) Y. Shiraishi, M. Itoh and T. Hirai, *Phys. Chem. Chem. Phys.*, 2010, **12**, 13737; b) J.-R. Chen and D.-Y. Yang, *Org. Lett.*, 2009, **11**, 1769.
- 13 a) M. E. Genovese, E. Colusso, M. Colombo, A. Martucci, A. Athanassiou and D. Fragouli, *J. Mater. Chem. A*, 2017, **5**, 339; b) J. T. C. Wojtyk, A. Wasey, N.-N. Xiao, P. M. Kazmaier, S. Hoz, C. Yu, R. P. Lemieux and E. Bunzel, *J. Phys. Chem. A*, 2007, **111**, 2511.
- 14 a) M. Baldrighi, G. Locatelli, J. Desper, C. B. Aakeröy and S. Giordani, *Chem. Eur. J.*, 2016, **22**, 13976; b) K. H. Fries, J. D. Driskell, G. R. Sheppard and J. Locklin, *Langmuir*, 2011, **27**, 12253.
- 15 a) H. Zhang, Y. Chen, Y. Lin, X. Fang, Y. Xu, Y. Ruan and W. Weng, *Macromolecules*, 2014, **47**, 6783; b) X. Meng, G. Qi, X. Li, Z. Wang, K. Wang, B. Zou and Y. Ma, *J. Mater. Chem. C*, 2016, **4**, 7584.
- 16 a) N. Murase, T. Mukawa, H. Sunayama, T. Takeuchi, *J. Polym. Science, Part B: Polymer Physics*, 2016, **54**, 1637; b) L. Kortekaas, O. Ivashenko, J. T. van Herpt and W. R. Browne, *J. Am. Chem. Soc.*, 2016, **138**, 1301; c) Y. Zhang, M. Cao, B. Yuan, T. Guo and W. Zhang, *Polym. Chem.*, 2017, **8**, 7325.
- 17 a) F. Nickel, M. Bernien, K. Kraffert, D. Krüger, L. M. Arruda, L. Kippen and W. Kuch, *Adv. Funct. Mater.*, 2017, **27**, 1702280; b) A.-R. Jang, E. K. Jeon, D. Kang, G. Kim, B.-S. Kim, D. J. Kang and H. S. Shin, *ACS Nano*, 2012, **6**, 9207; c) O. Ivashenko, J. T. van Herpt, B. L. Feringa, P. Rudolf and W. R. Browne, *Langmuir*, 2013, **29**, 4290.
- 18 a) P. K. Kundu, S. Das, J. Ahrens and R. Klajn, *Nanoscale*, 2016, **8**, 19280; b) A. Abdollahi, A. R. Mahdavian and H. Salehi-Mobarakeh, *Langmuir*, 2015, **31**, 10672; c) Y. Shiraishi, E. Shirakawa, K. Tanaka, H. Sakamoto, S. Ichikawa and T. Hirai, *ACS Appl. Mater. Interfaces*, 2014, **6**, 7554.
- 19 a) Y. Okabe and M. Ogawa, *RSC Adv.*, 2015, **5**, 101789; b) K. Kinashi, S. Nakamura, M. Imamura, K. Ishida and Y. Ueda, *J. Phys. Org. Chem.*, 2012, **25**, 462.
- 20 a) H. A. Schwartz, S. Olthof, D. Schaniel, K. Meerholz and U. Ruschewitz, *Inorg. Chem.*, 2017, **56**, 13100; b) K. Healey, W. Liang, P. D. Southon, T. L. Church and D. M. D'Alessandro, *J. Mater. Chem. A*, 2016, **4**, 10816; c) P. K. Kundu, G. L. Olsen, V. Kiss and R. Klajn, *Nature Communications*, 2014, **5**, 3588.
- 21 a) S. Bénard and P. Yu, *Adv. Mater.*, 2000, **12**, 48; b) B. Mondal, A. K. Ghosh and P. S. Mukherjee, *J. Org. Chem.*, 2017, **82**, 7783.
- 22 J. Harada, Y. Kawazoe and K. Ogawa, *Chem. Commun.*, 2010, **46**, 2593.
- 23 a) H. Lv, Y. V. Geletii, C. Zhao, J. W. Vickers, G. Zhu, Z. Luo, J. Song, T. Lian, D. G. Musaev and C. L. Hill, *Chem. Soc. Rev.*, 2012, **41**, 7572; b) S.-S. Wang and G.-Y. Yang, *Chem. Rev.*, 2015, **115**, 11, 4893; c) I. A. Weinstock, R. E. Schreiber and R. Neumann, *Chem. Rev.*, 2018, **118**, 2680.
- 24 a) T. Yamase, *Chem. Rev.*, 1998, **98**, 307; b) J. Xu, H. Volfova, R. J. Mulder, L. Goerigk, G. Bryant, E. Riedle, and C. Ritchie, *J. Am. Chem. Soc.*, 2018, **140**, 10482; c) P. Ma, F. Hu, R. Wan, Y. Huo, D. Zhang, J. Niu and J. Wang, *J. Mater. Chem. C*, 2016, **4**, 5424; d) L. Li, J.-R. Wang, Y. Hua, Y. Guo, C. Fu, Y.-N. Sun and H. Zhang, *J. Mater. Chem. C*, 2019, **7**, 38; e) J. Wang, P. Ma, S. Li, Q. Xu, Y. Li, J. Niu and J. Wang, *Inorg. Chem.*, 2019, **58**, 57; f) A. Al-Yasari, P. Spence, H. El Moll, N. Van Steerteghem, P. N. Horton, B. S. Brunschwig, K. Clays and J. Fielden, *Dalton Trans.*, 2018, **47**, 10415.
- 25 K. Hakouk, O. Oms, A. Dolbecq, J. Marrot, A. Saad, P. Mialane, H. El Bekkachi, S. Jobic, P. Deniard and R. Dessapt, *J. Mater. Chem. C*, 2014, **2**, 1628.
- 26 P. Mialane, G. Zhang, I. M. Mbomekalle, Pei Y., J.-D. Compain, A. Dolbecq, J. Marrot, F. Sécheresse, B. Keita and L. Nadjo, *Chem. Eur. J.*, 2010, **16**, 5572.
- 27 O. Oms, K. Hakouk, R. Dessapt, P. Deniard, S. Jobic, A. Dolbecq, T. Palacin, L. Nadjo, B. Keita, J. Marrot and P. Mialane, *Chem. Commun.*, 2012, **48**, 12103.
- 28 A. Saad, O. Oms, A. Dolbecq, C. Menet, R. Dessapt, H. Serier-Brault, E. Allard, K. Baczkko and P. Mialane, *Chem. Commun.*, 2015, **51**, 16088.
- 29 Y. Chu, A. Saad, P. Yin, J. Wu, O. Oms, A. Dolbecq, P. Mialane and T. Liu, *Chem Eur. J.*, 2016, **22**, 11756.
- 30 A. Saad, O. Oms, J. Marrot, A. Dolbecq, K. Hakouk, H. Rl Bekkachi, S. Jobic, P. Deniard, R. Dessapt, D. Garrot, K. Boukheddaden, R. Liu, G. Zhang, B. Keita and P. Mialane, *J. Mater. Chem. C*, 2014, **2**, 474.
- 31 A. Parrot, A. Bernard, A. Jacquart, S. A. Serapian, C. Bo, E. Derat, O. Oms, A. Dolbecq, A. Proust, R. Métivier, P. Mialane and G. Izzet, *Angew. Chem. Int. Ed.*, 2017, **56**, 4872.
- 32 H. Ai, Y. Wang, B. Li and L. Wu, *Eur. J. Inorg. Chem.*, 2014, **17**, 2766.
- 33 A. Fissi, O. Pieroni, G. Ruggeri and F. Ciardelli, *Macromolecules*, 1995, **28**, 302.
- 34 a) D. Shevchenko, P. Huang, V. V. Bon, M. F. Anderlund, V. N. Kokozay, S. Styring and A. Thapper, *Dalton Trans.*, 2013, **42**, 5130; b) H. M. Asif, Y. Zhou, L. Zhang, N. Shaheen, D. Yang, J. Li, Y. Long, A. Iqbal and Y. Li, *Inorg. Chem.*, 2017, **56**, 9436; c) S. R. Amanchi, A. M. Khenkin, Y. Diskin-Posner and R. Neumann, *ACS Catal.*, 2015, **5**, 3336.
- 35 X. Li, Y. Wang, T. Matsuura and J. Meng, *Heterocycles*, 1999, **51**, 2639.
- 36 S. Vanhaecht, T. Quanten and T. N. Parac-Vogt, *Dalton Trans.*, 2017, **46**, 10215.
- 37 a) H. Zeng, G. R. Newkome and C. L. Hill, *Angew. Chem. Int. Ed.*, 2000, **39**, 1772; b) C. P. Pradeep, D.-L. Long, G. N. Newton, Y.-F. Song and L. Cronin, *Angew. Chem. Int. Ed.*, 2008, **47**, 4388; c) Y. Han, Y. Xiao, Z. Zhang, B. Liu, P. Zheng, S. He and W. Wang, *Macromolecules*, 2009, **42**, 6543; d) M. F. Misdrhi, M. Wang, C. P. Pradeep, F.-Y. Li, C. Lydon, L. Xu, L. Cronin and T. Liu, *Langmuir*, 2011, **27**, 9193; e) M.-P. Santoni, A. K. Pal, G. S. Hanan, A. Proust and B. Hasenknopf, *Inorg. Chem.*, 2011, **50**, 6737; f) C. Allain, D. Schaming, N. Karakostas, M. Erard, J.-P. Gisselbrecht, S. Sorgues, I. Lampre, L. Ruhlmann and B. Hasenknopf, *Dalton Trans.*, 2013, **42**, 2745; g) I. Alzcarate, I. Ahmed, R. Farha, M. Goldmann, X. Wang, H. Xu, B. Hasenknopf, E. Lacôte and L.

- Ruhlmann, *Dalton Trans.*, 2013, **42**, 12688; h) P. Yin, T. Li, R. S. Forgan, C. Lydon, X. Zuo, Z. N. Zheng, B. Lee, D. Long, L. Cronin and T. Liu, *J. Am. Chem. Soc.*, 2013, **135**, 13425; i) J. Tang, W. Yu, M.-B. Hu, Y. Xiao, X.-G. Wang, L.-J. Ren, P. Zheng, W. Zhu, Y. Chen and W. Wang, *ChemPlusChem*, 2014, **79**, 1455; j) B. Zhang, C. P. Pradeep, L. Cronin and T. Liu, *Chem. Commun.*, 2015, **51**, 8630; k) V. Kalyani, V. S. V. Satyanarayana, V. Singh, C. P. Pradeep, S. Ghosh, S. K. Sharma and K. E. Gonsalves, *Chem. Eur. J.*, 2015, **21**, 2250; l) W. Chen, U. Tong, T. Zeng, C. Streb and Y.-F. Song, *J. Mater. Chem. C*, 2015, **3**, 4388; m) C. Ma, H. Wu, Z.-H. Huang, R.-H. Guo, M.-B. Hu, C. Kübel, L.-T. Yan and W. Wang, *Angew. Chem. Int. Ed.*, 2015, **54**, 15699; n) T. Auvray, M.-P. Santoni, B. Hasenknopf and G. S. Hanan, *Dalton Trans.*, 2017, **46**, 10029; o) H. M. Asif, Y. Zhou, L. Zhang, N. Shaheen, D. Yang, J. Li, Y. Long, A. Iqbal and Y. Li, *Inorg. Chem.*, 2017, **56**, 9436.
- 38 J. Li, I. Huth, L.-M. Chamoreau, B. Hasenknopf, E. Lacôte, S. Thorimbert and M. Malacria, *Angew. Chem. Int. Ed.*, 2009, **48**, 2035.
- 39 a) O. Ivashenko, J. T. van Herpt, B. L. Feringa, P. Rudolf and W. R. Browne, *J. Phys. Chem. C.*, 2013, **117**, 18567; b) O. Ivashenko, J. T. van Herpt, P. Rudolf, B. L. Feringa and W. R. Browne, *Chem. Commun.* 2013, **49**, 6737.
- 40 Y. Hou and C. L. Hill, *J. Am. Chem. Soc.*, 1993, **115**, 11823.
- 41 K. Horie, M. Tsukamoto, I. Mita, *Eur. Polym. J.*, 1985, **21**, 805.
- 42 V. M. Breslin, M. A. Garcia-Garibay, *Cryst. Growth Des.*, 2017, **17**, 637.
- 43 S. B. Anantharaman, S. Yakunin, C. Peng, M. Vinícius Gonçalves Vismara, C. F. O. Graeff, F. A. Nüesch, S. Jenatsch, R. Hany, M. V. Kovalenko and J. Heier, *J. Phys. Chem. C.*, 2017, **121**, 9587.
- 44 P. Bolle, Y. Chéret, C. Roiland, L. Sanguinet, E. Faulques, H. Serier-Brault, P.-A. Bouit, M. Hissler and R. Dessapt, *Chem. Asian J.*, 2019, **14**, 1642.
- 45 B. Matt, X. Xiang, A. L. Kaledin, N. Han, J. Moussa, H. Amouri, S. Alves, C. L. Hill, T. Lian, D. G. Musaev, G. Izzet and A. Proust, *Chem. Sci.*, 2013, **4**, 1737.
- 46 D. Schaming, C. Allain, R. Farha, M. Goldmann, S. Lobstein, A. Giraudeau, B. Hasenknopf and L. Ruhlmann, *Langmuir*, 2010, **26**, 5101.
- 47 S. Schönweiz, M. Heiland, M. Anjass, T. Jacob, S. Rau and C. Streb, *Chem. Eur. J.*, 2017, **23**, 15370.
- 48 R. G. Finke, B. Rapko, R. J. Saxton, P. J. Domaille, *J. Am. Chem. Soc.*, 1986, **108**, 2947.